Spring 1-1-2014

Regeneration of Liquid Desiccants in Evacuated Tube Solar Collectors

Darrell J. Hubler
University of Colorado at Boulder, djhubler@gmail.com

REGENERATION OF LIQUID DESICCANTS IN EVACUATED TUBE SOLAR COLLECTORS

by

DARRELL JAMES HUBLER

B.S., Oregon State University, 2003

A thesis submitted to the
Faculty of the Graduate School of the
University of Colorado in partial fulfillment
of the requirement for the degree of
Master's of Science
Department of Civil, Environmental and Architectural Engineering
2014

This thesis entitled:

Regeneration of Liquid Desiccants in Evacuated Tube Solar Collectors written by Darrell James Hubler

has been approved for the Department of Civil Environmental and Architectural Engineering

_____

Dr. Michael Brandemuehl

_____

Dr. Moncef Krarti

Date_____

The final copy of this thesis has been examined by the signatories, and we find that both the content and the form meet acceptable presentation standards of scholarly work in the above mentioned discipline.

ABSTRACT

Hubler, Darrell James (M.S. Architectural Engineering Department of Civil, Environmental and Architectural Engineering)

Regeneration of Liquid Desiccants in Evacuated Tube Solar Collectors

Thesis Directed by Professor Michael Brandemuehl

Liquid desiccants can be regenerated by heating the solution to evaporate water from the solution. While conventional methods rely on the vapor pressure difference between water in the solution and that in moist air, it has been proposed to directly boil the desiccant in evacuated tube solar collectors. Regeneration by boiling makes the evacuated tube regenerator less susceptible to performance decreases due to humid weather. The low thermal loss through the walls of the evacuated tube also allows regeneration in colder climates.

An experimental study was conducted to characterize the opportunity to directly regenerate liquid desiccants in evacuated tube solar collectors. Measurements were performed on a single tilted evacuated tube during outdoor tests using solutions of calcium chloride and water at nominal mass fractions of 10%, 30%, and 50%. The amount of water evaporated from a desiccant solution was determined by measuring both the change in mass of a solution and the mass of water evaporated during regeneration. The test apparatus was further instrumented to provide incident solar radiation on the tube and transient solution temperature measurements inside the collector tube. Test results indicated that the desiccant could be regenerated without significant concentration stratification in the tube.

A model of the collector tube was developed, based on well-established efficiency relationships for solar collectors that relate useful energy production to the incident solar radiation and the thermal

losses. Using model parameters identified by the experimental data, the model was demonstrated to effectively predict desiccant regeneration rates. The results suggest that regeneration performance can be predicted using simple models with conventional collector efficiency curves.

DEDICATION

This thesis is dedicated to my wife Katy. Thank you for all of the love, support and patience through the process of writing and correcting this thesis.

ACKNOWLEDGEMENTS

I would like to acknowledge my thesis committee: Dr. Michael Brandemuehl, Dr. Jay Burch and Dr. Moncef Krarti who all, in their own way provided insight and questions; helped push though many barriers along the process of completing this work; taught me to pay attention to details and understand experimental design and the beauty of a good data set; and provided realistic view and sense of the bigger picture.

TABLE OF CONTENTS

LIST OF FIGURES

1 INTRODUCTION AND LITERATURE REVIEW

1.1 Introduction

Solar thermal collectors have been well studied over the years. In general, they are effective at collecting heat from the sun for use in buildings. The problem with solar thermal collectors is that they collect the most heat in the warm summer months when that heat has little or no use. In order to best utilize the heat collected from a solar thermal system, especially if loads such as space heating are to be met with the system, a storage system is needed.

Standard thermal storage systems use sensible heat in a relatively high heat capacity substance such as water, glycol, rocks, or the ground to store heat. There are two main problems with this type of heat storage. The first problem is that storing sensible heat requires a tremendous volume or storage capacity to store the heat collected in the summer for use in the winter for space heating. The second problem with sensible heat storage is that no matter how well the system is insulated, there will be thermal losses.

On the other hand thermal-chemical storage, which utilizes chemical potential energy, can store similar amounts of thermal potential as thermal storage with a fraction of the required volume. If designed correctly, thermal-chemical storage can store energy with little or no losses to the ambient. The thermal-chemical substance under investigation here is an aqueous desiccant solution of Calcium Chloride ($CaCl_2$). Desiccants, in contact with moisture, will absorb the moisture and increase in temperature. This temperature increase comes from the heat of condensation released when water vapor condenses into the solution. A stored volume of concentrated desiccant solution can therefore act as a thermal storage. As a result of absorption however, the desiccant becomes less concentrated and therefore less effective. A way to regenerate this desiccant is needed. The topic of this paper is the regeneration of liquid desiccants in evacuated tube solar collectors and the creation of a model that will predict regeneration performance.

1.2 Desiccants and Desiccant Properties

As mentioned in section 1.1, strong liquid desiccants can be effective thermo-chemical storage mechanisms. The two most common desiccants that have been studied are calcium chloride and lithium chloride. In order to create a model that will predict regeneration performance, the thermo-physical properties of the solution need to be understood.

Conde (2004) completed a literature survey of measured data from 1850 to the present and developed calculation models based on correlations of the date reviewed. The majority of the correlations in Conde's study are based upon the mass fraction of the solution. Conde created correlations for the solubility boundary, vapor pressure, density, surface tension, dynamic viscosity, thermal conductivity, specific thermal capacity and differential enthalpy of dilution. Of particular interest in this study are; solubility boundary, vapor pressure, density, specific thermal capacity and differential enthalpy of dilution. The other properties are more suited for a study of the use of desiccants as a pumped heat transfer fluid.

Understanding that lithium chloride has preferable thermo-physical properties to calcium chloride but is significantly more expensive, Ertas (1992) proposed a mixture of the two solutions. As would be expected, the performance of the solution, based on the vapor pressure at a particular temperature and mass fraction, was better than that of pure calcium chloride, but worse than pure lithium chloride. Ertas concluded that the mixed solution could reach the same vapor pressure at a given temperature as pure lithium chloride at 30% reduced cost. In the study, Ertas also noted that the mixed solution could be more easily regenerated than a pure solution of lithium chloride.

1.3 Current Technologies for Regenerating Liquid Desiccants

There is an abundance of research into the regeneration of liquid desiccants. Essentially, liquid desiccant regeneration involves increasing the vapor pressure of the liquid desiccant above the ambient

vapor pressure of the surrounding air. As a result, water in the liquid desiccant solution is evaporated into the air and the desiccant solution left behind is more concentrated. Raising the vapor pressure of the liquid desiccant is generally accomplished by heating the desiccant solution. Since the desiccant does not have to reach extreme temperatures to regenerate, solar energy can be used to heat the solution. This section explains the method, pros and cons of some of the more popular methods of desiccant regeneration.

1.3.1 Open Flat Plates

Open flat plate desiccant regenerators were first studied by Kakabaev and Khandurdyev in the U.S.S.R (1969), and by Collier (1979). These flat plate regenerators are painted black and tilted. The desiccant that is to be regenerated is allowed to trickle down the tilted surface and water is evaporated from the solution, driven off by the hot black metal of the plate. There is a trough at the bottom of the collector surface into which the regenerated desiccant flows. From there it is cycled back through the desiccant refrigeration process to end up in the header at the top of the open regenerator to repeat the regeneration cycle.

Collier tested such a regenerator with a solution of lithium chloride under conditions of varying ambient temperature and humidity, wind speed, starting temperature of the desiccant prior to regeneration, initial concentrations of the desiccant and solar insolation. He found that the design of the collector was very dependent upon the relative humidity of the location in which regeneration was to occur. Using the ratio of solution flow rate per unit collector width to the collector length, Collier concluded that collector lengths needed for any kind of practical regeneration to occur would have to be very large. In dry climates however, more reasonable collector lengths could be designed. On top of the humidity problem, Collier noted that open regenerators were also susceptible to dust contaminating the solution and rainwater diluting the solution.

1.3.2 Closed Flat Plates

Closed flat plates, which have also been studied under the name of "tilted solar still" are better suited for use in humid climates than open regenerators. In addition to their improved performance in high humidity, these regenerators solve the problem of dust or rainwater entering the solution being regenerated. Closed flat plat regenerators work very similarly to their open flat plate cousins, the only difference is the addition of glazing above the collector surface. Figure 1-1 is a schematic of a typical closed desiccant regenerator for which Gandhidasan [6] conducted a numerical study.

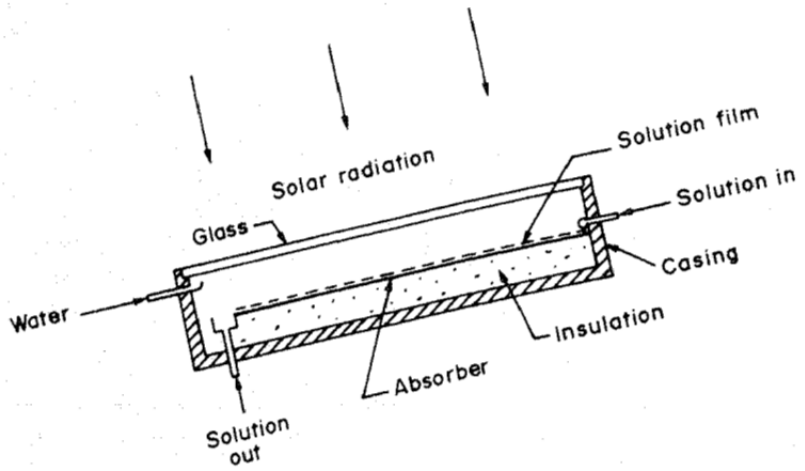

Figure 1-1: Schematic of a Tilted Solar Still (from (Gandhidasan 1983))

In this type of system, the water that is evaporated as the desiccant trickles down the tilted surface condenses on the underside of the glass cover and makes its way to a water removal tray at the bottom of the unit. In his numerical study, Gandhidasan calculated the amount of water evaporated from the solution as a function of the solar still area. Gandhidasan found that even at entering solution temperatures of 80 °C, the solar still was only able to evaporate water at a rate of 0.2 kg/m^2-h. This is around an order of magnitude less than the forced flow covered collector to which he was comparing the solar still. Gandhidasan concluded that the desiccant regeneration rate depends not only on the solution temperature,

but also on the potential for mass transfer, or, the difference in vapor pressure between the solution surface and the inside surface of the glazing. In this case, the mass transfer potential was reduced because the underside surface of the glazing was hot and therefore had a higher vapor pressure. Because of this a forced airflow regenerator will work better than a solar still in all but the most humid conditions. In addition to the evaporation rate, Gandhidasan also found that the optimum flow rate of the solution through the still increased with an increase in incident solar radiation.

1.3.3 Partially-Open, Partially Closed Flat Plates

Taking the results of his solar still study a bit further, Gandhidasan performed a similar theoretical analysis on a partially-open, partially closed solar still (Gandhidasan 1994). In this study, Gandhidasan examined the effects of insolation, ambient air temperature and ambient air vapor pressure on the performance of the regenerator based on the ratio of glazed area to open area. Performance was measured by an efficiency defined as the ratio of energy used to evaporate water from the unglazed surface to the total energy incident on both the glazed and unglazed surfaces. As would be predicted, highest efficiencies were seen at the highest ambient temperatures, greatest amount of insolation and smallest ambient water vapor pressure. For each situation however, there was an optimum ratio of glazed to unglazed area that changed with the conditions. Efficiencies ranged from 10%-25% for the range of conditions examined in the study. Gandhidasan concluded that this type of a regenerator could be used in humid climates, but in dryer, hotter climates, the addition of the glazing acts to reduce overall regeneration efficiency

1.3.4 Other Desiccant Regenerators

Packed bed and roof top pool regenerators have also been proposed and studied (Kim and Seo 2007) and (Radhwan et al 1993). In a packed bed regenerator, desiccant is dripped or sprayed over a packing material that increases the surface area for mass transfer. Air is blown counter to the flow of the

desiccant. Solar energy is used to heat the air/or desiccant prior to interaction in the packed bed chamber. Heating the two fluids allows for higher mass transfer rates and consequently better efficiency of the regenerator

The simplest of all regeneration methods is probably the desiccant roof pond. In this method, liquid desiccant is pooled on the roof of a building and water is evaporated simply through exposure to the sun. As with open flat plate regenerators, roof ponds are very sensitive to ambient humidity and wind conditions. They also allow dust into the desiccant solution as the ponds are typically uncovered.

Since neither roof ponds nor packed beds directly use solar collectors to regenerate desiccants, they are not readily applicable to the background discussion of this paper. They are included here simply as a background into other ways that desiccants are regenerated.

1.4 Case for Experiment

Section 1.3 described the most popular methods for regenerating liquid desiccants using solar energy. All of the methods described can be effective at regenerating desiccants depending on the ambient conditions. Open flat plates are very good at regeneration in dry, hot climates but do not work well when the ambient air is humid. Solar stills and partially-open, partially-closed flat plat regenerators do work with humid ambient air, but are less efficient than open flat plates when the air is hot and dry.
In addition to the dependence on ambient air conditions, the regenerators in Section 1.3 have other problems as well. Open flat plate regenerators can be exposed to dust which can contaminate the desiccant solution. Closed flat plate collectors can use fans to help increase their effectiveness, but this makes them more sensitive to the ambient conditions and fans create a parasitic loss on the overall system performance. All of the systems examined require fairly specific and somewhat complicated construction that does not allow collectors to be effectively mass produced. This keeps the cost of production high and limits the economic feasibility of using these regenerators and desiccant cooling more generally.

The case can then be made for a way to regenerate liquid desiccants that does not include the inherent downsides described in the previous paragraph. In this paper, a novel desiccant regeneration method using evacuated tube solar collectors is proposed and analyzed. In this study, desiccant is introduced to water-in-glass evacuated tubes, and brought to a boil while exposed to solar radiation. The tube is completely separated from the ambient conditions as the top of the tube is sealed off with a rubber stopper. Water vapor is allowed to escape via a Tygon tube. A more detailed description of the regenerator can be found in Section 2.2. The separation from the ambient reduces the dependence of regenerator performance on ambient conditions. On the other hand, regeneration through boiling increases the performance of the regenerator relative to closed solar stills as regeneration is no longer dependent on the relative vapor pressure inside the regeneration vessel. The following section gives a background on evacuated tubes and the methods used to analyze their performance. Subsequent chapters describe the system and the analysis method used to determine performance.

1.5 Characterization of Evacuated Tubes

Evacuated tubes, as their name suggests, utilize two, concentric glass tubes with the space between the two tubes evacuated to minimize thermal losses. Because the vacuum between the tubes is such an effective insulator, evacuated tubes can be used in cold climates and can achieve very high temperatures in warm conditions. It is for this reason that evacuated tubes were chosen to boil liquid desiccants.

The downside to evacuated tubes is that in warm climates they are less efficient overall than flat plate collectors. This is due mostly to the fact that when arranged into arrays, there are spaces between the tubes in which there is no absorber. Also unlike flat plate collectors where water is pumped through tubes and heat extracted from the absorber surface, removing heat from within the tube can be challenging. Further complicating the issue is the fact that in standard water heating applications, the glass walls of the tube are not strong enough by themselves to withstand the pressure of water mains. The

following section describes some solutions that have been proposed and analyzed to remove the heat from the evacuated tubes.

1.5.1 Types of Evacuated Tubes

A multitude of ways to extract the heat from the absorber surfaces of evacuated tubes have been studied in the past. Kim et al (2007) studied the effect of multiple types of copper absorbers inserted inside the clear inner tube of the evacuated apparatus. Figure 1-2 below depicts the absorber arrangements that were explored.

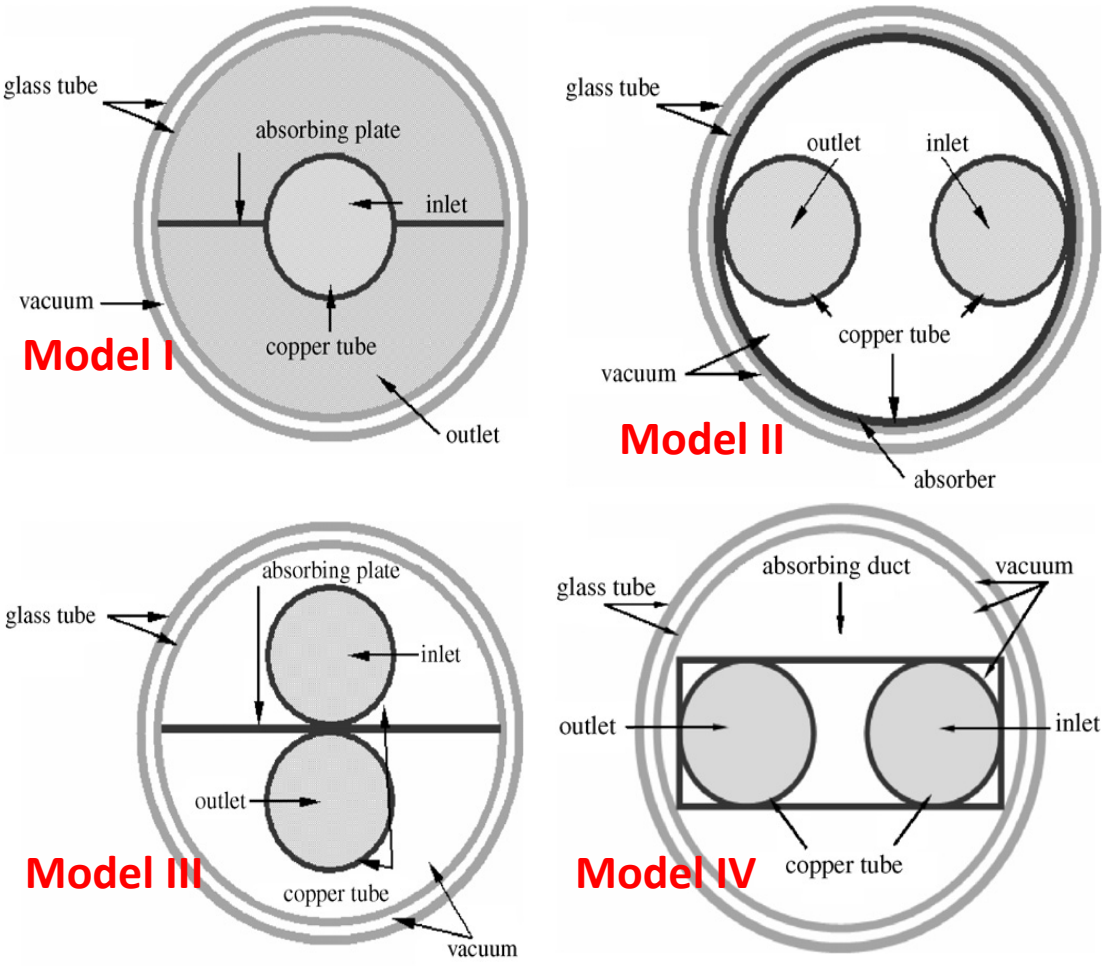

Figure 1-2: Evacuated Tube Absorber Arrangements Analyzed by Kim et al (2007)

In the figure, Model I is a copper tube going down the axis of the evacuated cylinder with a diametrical absorber attached to it. Fluid is pumped down the central copper tube and flows out of the tube along the outside of the central copper tube. Model II is simply a "U" shaped copper insert that is placed inside a cylindrical metal absorber immediately inside the inner glass tube. Fluid flows down one of the copper "U" legs and out the other. Model III is a "U" arrangement similar to Model II except that the legs of the "U" are attached to either side of a flat absorber plate. Model IV is again a "U" tube, this time it is circumscribed by a rectangular absorber. In all of these arrangements, it is important to note that the inner glass tube of the evacuated module is NOT used as an absorber.

Kim found that when the different models were tested individually with only beam radiation, Model III had the highest performance with small incidence angles. When the incidence angle increased, Model II started to have the best performance. Utilizing the shadow effects of tubular arrays and accounting for diffuse radiation, Model III had the best overall performance.

Harding et al (1995) conducted experiments on "U" tube arrangements similar to Model II of Kim. Harding however focused on arranging the "U" tubes into a manifold that would efficiently remove heat from an array of tubes. Harding concluded that manifolds that were closely coupled to the interior glass tube out-performed manifolds that weren't attached to the glass. Harding also proposed that the metal "U" tubes could be subject to corrosive effects.

Corrosion is a very big problem when regenerating liquid desiccants, especially if the desiccant solution is to be boiled. Boiling occurs at approximately 120 °C at concentrations in the 45% to 50% mass fraction range. At these temperatures copper, the typical metal used in evacuated tube manifolds, has been shown to have unacceptable resistance to corrosion in solutions of calcium chloride (Butler and Beynon 1967). For this reason and the fact that the addition of metal manifolds adds significant cost to the manufacture of evacuated tubes, water-in-glass evacuated tubes were selected to be tested as desiccant regenerators for study in this paper. A background on water-in-glass evacuated tubes follows.

1.5.2 Water-in-Glass Evacuated Tubes

Water-in-glass evacuated tubes utilize thermosiphons to extract heat from the absorber surface which is a coating applied to the outside of the interior glass tube of the evacuated assembly. Tubular thermosiphons for heat transfer were first proposed by Lighthill (1953) who studied them for use in cooling turbine blades. In his studies, Lighthill found that the ratio of tube diameter to tube length had a large effect on the ability of thermosiphons to form in tubes. At small diameter to length ratios, Lighthill found that the bottom of the single open ended tube stagnated and the thermosiphon would not extend for the entire length of the tube.

Thermosiphons in water-in-glass evacuated tubes have been extensively studied by Morrison and Budihardjo (Morrison et al 2004) and (Budihardjo et al 2007). First, Morrison performed numerical studies on flow through single open ended tubes and found similar results to those published by Lighthill. Budihardjo, using a combination of particle velocimetry and computational fluid dynamics related the mass flow rate into and out of the tube; to tube angle, incident solar radiation and aspect ratio of the tube. This relation was used to create a computer model that would predict the annual performance of an array of evacuated tube solar collectors. This theoretical model was then tested against an actual evacuated tube array and shown to match well. Using the model for a variety of climate zones, Budihardjo concluded that evacuated tubes worked very well in most climates and the simplified design of water-in-glass evacuated tubes makes this solar collector a viable economic alternative to flat plates. The favorable performance results of Budihardjo's study lend more weight to the theory of regenerating liquid desiccants in water-in-glass evacuated tubes. Before describing this study however, a brief background on the differences in calculating incident solar radiation between flat plates and evacuated tubes should be given.

1.5.3 Calculating Incident Radiation on Evacuated Tubes

Calculating incident solar radiation on a tilted plane is well understood and straightforward. Readily available solar data typically includes global horizontal, direct normal and diffuse horizontal. Using this

common solar data, Perez (1995) provides a method for calculating the incident radiation on a collector with tubular geometry. This process will be explained in much more detail in Section 4.3.4. The difference to keep in mind while comparing incidence angles on flat plates versus tubes is that tubes having cylindrical collector surfaces act like a single axis tracking collector which rotates about the axis of the tube. This makes the incidence angle on a tube solely the angle between a line perpendicular to the axis of the tube in a plane that contains the axis of the tube and the sun. What this practically does is allow the tube to collect much more solar radiation in the morning and afternoon hours because the tube is effectively acting like a flat plate with the normal of the plane pointing nearly directly at the sun.

2 EXPERIMENTAL SETUP AND PROCEDURE

2.1 Introduction

An experimental apparatus was constructed to test the feasibility of directly boiling liquid desiccants in an evacuated tube. A fixed volume of different mass fractions of an aqueous solution of calcium chloride was poured in the tube and allowed to heat up and boil while exposed to solar radiation. The mass of the solution was measured both before and after boiling in the tube. The difference in mass was the amount of water boiled and consequently the amount of desiccant regeneration that had occurred.

Thermocouples placed equidistantly along the axis of the tube measured the temperature of the solution in the tube as a function of time as the solution was heating up prior to boiling. The temperature increase over time, in conjunction with solar radiation was used to characterize the performance of the evacuated tube. The performance characteristics of the tube along with measured solar radiation and material properties of the liquid desiccant was used to create a model that predicts the magnitude of regeneration. The directly measured experimental results were used to calibrate and validate the model. This section explains in further detail the experimental apparatus and procedure used to both directly measure and model regeneration of desiccant in the evacuated tube.

2.2 Apparatus

2.2.1 Evacuated Tube Collector and Frame

Figure 2-1 shows a photo of the apparatus in situ on the roof of the Thermal Test Facility at the National Renewable Energy Lab in Golden Colorado. The roof faces South at a tilt angle of 27.5°. The roof surface is standard asphalt shingle with a reflectance of 0.1 which is the average for composite shingles. A Sun Maxx water-in-glass evacuated tube was mounted to the roof with a wooden frame. The

tube was 1.8m long and 0.0577m in outside diameter. The diameter of the inner tube upon which the selective coating resides was 0.047m. This dimension is important as it is the diameter used in calculating absorber area. The two-part wooden frame was attached at the top and bottom of the tube with hose clamps. Between the hose clamps and the tube were thin strips of rubber used to keep the tube secure in the hose clamps. The wooden frame attached to the top of the tube was hinged, which allowed the tube to pivot without unscrewing the frame from the roof. The frame at the bottom of the tube latched with quick-release metal hooks that attached the tube to the roof during experimentation but could be released to allow the tube to pivot and pour out solution when testing was complete. The white object at the top of the tube was pipe insulation cut to a length of 33.64 cm. This length of pipe insulation allowed the level of the solution in the tube to drop by 500 ml during regeneration and maintained the same effective collector area. In none of the experimental trials did the level inside the tube drop below the level of the pipe insulation.

Figure 2-1: Experimental Setup

Figure 2-1 shows the bottom of the evacuated tube with the hose clamp and the latches that keep the tube secure to the roof when testing. After the solution had boiled in the tube, the latches were released so that the tube tilted to allow the regenerated desiccant to pour out.

Figure 2-2: Close-up of Bottom of Tube and Frame

Figure 2-3 shows a close-up of the top of the tube. The green rubber stopper sealed the interior chamber of the tube from the ambient. Tygon tubing and thermocouple wires can be seen coming out of the rubber stopper. The Tygon tubing carried the water vapor to the condensing coil and the hole where the thermocouple wires penetrated the rubber stopper is sealed with silicone caulking. The hinge that allowed the tube to pivot and pour out its solution can also be seen in Figure 2-3.

Figure 2-3: Close-up of Top of Tube

2.2.2 Condensing Coil and Condensate Collection

Figure 2-4 shows the system that was used to condense the water vapor that had been boiled inside the evacuated tube and collected for direct measurement. In the upper left-hand corner of the figure the Tygon tube described in Figure 2-3 can be seen connected to the top of a copper coil inside of a blue bucket. The 4.76 mm outside diameter copper coil was placed inside the bucket so that cold water could be used to condense the water faster. Any water vapor that had not been condensed by the time it reaches the copper coil would condense in the coil and drip into the volumetric flask below. The volumetric flask was Pyrex and measured a volume of 500 ml. Aluminum foil was wrapped around the interface of the copper tubing and the mouth of the volumetric flask during experimentation to limit and condensate re-evaporating after it had condensed. This aluminum foil is not shown in the figure for clarity. Figure 2-5 shows a close-up of the copper coil inside the bucket and the connection of the Tygon tube to the copper coil.

Figure 2-4: Vapor Condensate and Collection Apparatus

Figure 2-5: Close-up of Copper Coil in Bucket

2.2.3 Instrumentation

Figure 2-6 shows the thermocouple placement inside the apparatus. There are five evenly spaced thermocouples along the axis of the tube. The thermocouples are attached to a 4.76 mm polycarbonate rod positioned directly in the center of the tube by polycarbonate "legs" that rest on the bottom of the inside of the tube. Figure 2-7 depicts the polycarbonate legs used to hold the thermocouples in the center of the tube. The diameter of the hole in the center of the leg piece was equivalent to 1/16 of an inch. The lengths of the legs were the radius of the inside of the inner tube ensuring that the polycarbonate rod was precisely in the center of the tube.

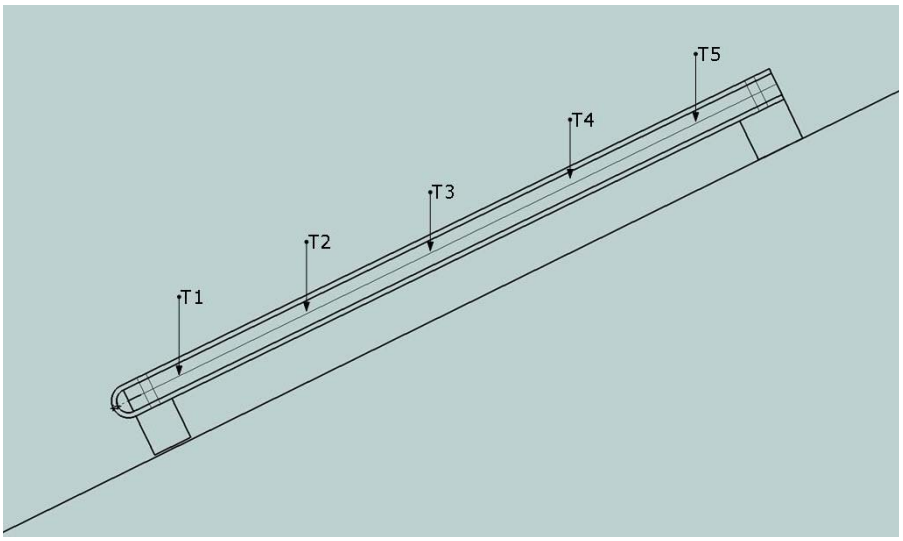

Figure 2-6: Thermocouple Layout

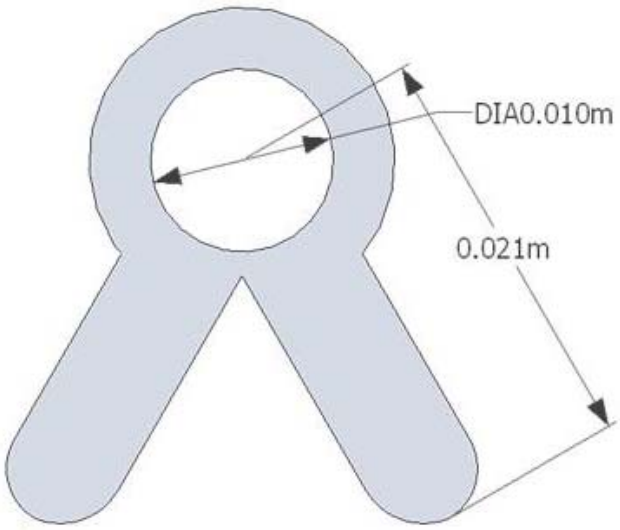

Figure 2-7: Picture of Polycarbonate "Legs"

The thermocouples used in this experiment are 24 gauge TC high tolerance thermocouples attached to a data acquisition unit set to collect temperature data every minute. The thermocouple junctions were made by twisting the two exposed wires together and then soldered. After the solder had

cooled, the junctions were potted with 3M DP 270 potting compound. This potting compound was to keep the corrosive solution off of the metallic thermocouple junction. The temperatures present in this experiment were at the limit of the DP 270 but the thermocouple junctions appeared to be in good shape after the experiment. Subsequent testing of the thermocouples, discussed below, after the experiment showed that there was no adverse effect to the accuracy of the thermocouples.

After the thermocouples were soldered and potted, they were tested for accuracy by placing them in an ice water bath and measuring the temperature multiple times. Subsequently they were placed in a bath of boiling water and again took a series of temperature measurements. The overall uncertainty for all of the thermocouples at a 95% confidence is 0.211 °C. Bias error was found to be negligible.

2.3 Data Collection Methodology

Once the experimental apparatus was assembled, data could be collected. The methodology for collecting data is detailed in the following sub-sections. Prior to that, a brief overview of the methodology used to collect data is needed.

First a solution of calcium chloride was mixed to the desired nominal mass fraction. Mass fractions of 10%, 30% and 50% were examined in this study. The solution was poured inside the evacuated tube in 2450 ml batches that were at ambient temperature approximately two hours before solar noon. Pouring the solution into the tube two hours prior to solar noon would allow the solution to reach boiling near solar noon. Temperature data collected as the solution was heating up was used to predict collector behavior after the solution was boiling. All of the tests occurred between September 26 and October 7, 2009. The tests required perfectly sunny days as rapid fluctuations in solar radiation could not be predicted by the model.

The methodology presented in this section sets out to determine the amount of water boiled in three different ways. The first was by direct measurement of the change in mass of the solution prior to

regeneration as compared to after regeneration. The second was to capture, condense and measure the water vapor that was evaporated as the solution was regenerating. The third method of predicting the amount of water evaporated during regeneration was to collect solar radiation, ambient temperature, and solution temperature during the heat up phase of the solution, and use this data to create a model that would predict tube efficiency. Tube efficiency was used in conjunction with the thermodynamic properties of the solution to predict the amount of water evaporated

2.3.1 Initial Solution Preparation

Prior to the solution being introduced to the evacuated tube, it had to be mixed to the correct nominal mass fraction. This was accomplished by adding amounts of granular calcium chloride crystals to de-ionized water. The mass of a 500 ml sample was taken as well as the temperature and used to find the density of the solution. From the relations published by Conde [1], the mass fraction of the solution could be determined by the density and temperature of the solution. If the solution was not at the desired nominal mass fraction, more calcium chloride or more water was added to the solution.

Once the solution was at the desired mass fraction, five 500 ml samples were weighed in a 500 ml volumetric flask concurrently with the temperature of the sample being measured. The resulting five density values and temperatures could be used to determine the solution mass fraction. The five samples were taken to determine the statistical significance of the mass fraction value. Once this was accomplished, a 2450 ml batch was separated and weighed. This mass is the initial mass that was compared to the solution removed from the tube after regeneration.

2.3.2 Introduction and Removal of Solution into Tube

After being prepared to the desired mass fraction, the batch of solution was carried to the apparatus in a 10 liter plastic jug. The rubber stopper and thermocouple rod were removed from inside the evacuated tube and the solution was poured into the tube with the help of a large, spill resistant funnel.

After all of the solution was inside the tube, the thermocouples and rubber stopper were replaced and the tube was allowed to heat up in the sun. After the solution had boiled and the experiment completed, the rubber stopper and thermocouple rod were again removed from the evacuated tube. The large funnel was placed inside the opening to the plastic jug. The two latches on the bottom of the evacuated tube frame were released and the tube was tipped and the solution was poured through the funnel into the jug. Care was taken to avoid spilling solution as the final mass of the solution would no longer be accurate. The jug was taken from the apparatus to a scale where the final mass of solution was directly measured.

2.3.3 Temperature Measurement

While the solution was heating up and boiling inside the evacuated tube, the temperature of the solution was being measured at one minute intervals by five thermocouples. Each of the 5 thermocouples represented an equal volume of the solution inside of the evacuated tube. Budihardjo (2007) showed that thermocouples placed along the axis of the evacuated tube measured accurately the average representative temperature of that sub-volume of solution

2.3.4 Condensate Measurement

Utilizing the copper condensing coil, water vapor, created by boiling inside the evacuated tube was condensed and dripped into the volumetric flask. After the experiment was completed and the rubber stopper and thermocouple rod removed from the evacuated tube, the remaining water inside the coil was forced out with a small amount of air pressure applied to one end of the Tygon tubing. After all of the condensate had been emptied from the condensing coil, the volumetric flask was weighed to determine the mass of condensate. The mass of condensate should be equal to the difference in the initial mass of the solution and the final mass of the solution

2.3.5 Final Solution Analysis

Besides directly measuring the final mass of the solution after boiling, the mass, volume and temperature of samples of solution were taken as well. These measurements were used to determine the final solution density and mass fraction. This mass fraction was compared to the mass fraction from directly measuring the final mass of the solution.

3 PRELIMINARY ANALYSIS

Temperature measurements of the fluid in the tube were performed using a single set of thermocouples along the axis of the tube, centered in the tube at five axial locations. There is some concern that a single thermocouple at each axial position is not sufficient to accurately determine the average temperature for that section of evacuated tube. On the other hand, additional thermocouples could alter the flow field of the solution in the tube. This study intends to model the temperature profile inside the tube during a heat-up phase and determine if, indeed, a single thermocouple is sufficient.

3.1 CFD Analysis

Much research has been conducted into natural convection in enclosures. Of particular importance, is the work performed by Lighthill (1953). In his research, Lighthill examined natural convective flows in single open ended tubes. He proposed three types of flow regimes exist in the tube depending on the Rayleigh number and the aspect ratio of the tube's radius to the tube's length. The flow regimes are; developing flow when the heat flux is low enough that a thermosiphon is not yet formed, fully developed flow where there is a consistent thermosiphon throughout the tube, and short circuit flow where the aspect ratio is too small and a portion at the bottom of the tube is short circuited from the natural circulation. Behnia and Morrison later proved Lighthill's theories using flow visualization, Behnia and Morrison (1991)

In regards to computational models of this natural convective flow, Gosman et al (1971) used one of the first finite difference techniques to predict laminar flow in an open thermosiphon. Chan and Tien (1985) took this a step further when they modeled the two dimensional natural convective flow in an open square cavity. The side opposite the cavity opening was modeled as being heated in this case which is not directly relevant to the flow inside of an evacuated tube where the heated surface is adjacent to the cavity

opening. There have been numerous other numerical studies involving natural convection in cavities with different permutations of the shape and configuration of the cavity. Budihardjo et al (2005) created a CFD model of a dewar type evacuated tube. In her numerical study, Budihardjo modeled the effect of tube angle and input radiation on the effective flow rate through the tube opening. This numerical model was validated using particle velocimetry to measure the actual flow rate through the tube opening. Unlike most of the previous numerical studies, Budihardjo's model was three dimensional and considered radiation from all sides around the tube in various configurations.

Although some of the studies listed above were validated with experimental data, none of them were validated using temperature measurements. Also, all of the studies listed above were considered only in steady state. There was no attempt to determine the changes in conditions inside the computational domain as a function of time. Thusly, the objective of this numerical study is threefold:

1. Use temperature measurements to validate the numerical model and determine if a single thermocouple is sufficient to measure accurately the temperature inside the tube.

2. Compare velocity profiles of this computer model to the profiles provided by Budihardjo.

3. Perform a transient simulation of the calibrated CFD model and compare the rate of temperature increase inside the tube over one hour to the measured experimental temperature increase.

3.1.1 CFD Methodology

In general computational fluid dynamics software solves the general transport equation given by,

$$\frac{\partial \rho \phi}{\partial t} + \frac{\partial \rho U_j \phi}{\partial x_j} = \frac{\partial}{\partial x_j}\left(\Gamma_\theta \frac{\partial \phi}{\partial x_j}\right) + S_\theta \qquad (3\text{-}1)$$

Where ϕ is the transported quantity, t is time, U_j is the Einsteinian representation of velocity in the three dimensions, x_j is the Einsteinian position in three dimensions, Γ_θ is the transport property of the given ϕ and S_θ is the source term of the given transported quantity. For this case, the general transport equation is used in three forms; replacing ϕ with 1 gives the mass equation, replacing ϕ with U_i gives the momentum equation, and replacing ϕ with T gives the temperature equation. Please note that whilst changing ϕ the transport property Γ_θ will change as well.

The commercial CFD software Phoenics was used to solve these transport equations simultaneously. For this case, the HYBRID differencing scheme was used.

3.1.1.1 Turbulence and Buoyancy Models

For the tubular model performed by Budihardjo (2005) a laminar flow was used. This approach is reasonable given that the Grashof number for this flow given by,

$$Gr_L = \frac{g\beta(T_s - T_\infty)L^3}{\nu^2} \qquad (3\text{-}2)$$

is 12.35 for this case which is well below the transitional region that starts with Grashof numbers around 3,000,000. Behzadmehr et al (2002). For this case, therefore, laminar flow is predicted and no turbulence model is needed.

Due to the low expected temperature differences in the flow domain. It is reasonable to assume that there will be relatively low density differences and therefore the Boussinesq buoyancy approximation is valid.

3.1.2 CFD Case Description

The CFD model was set up to predict behavior of the experimental apparatus at solar noon. Measurements showed that solar radiation at this time was around 1000 W/m2 while the ambient temperature was 14 °C. The tube was at an angle of 40° which is depicted in Figure 3-1 below. The simulation was run as a one hour transient starting with a fluid temperature of 40 °C. The simulation was run for 50,000 iterations.

3.1.3 Boundary Conditions

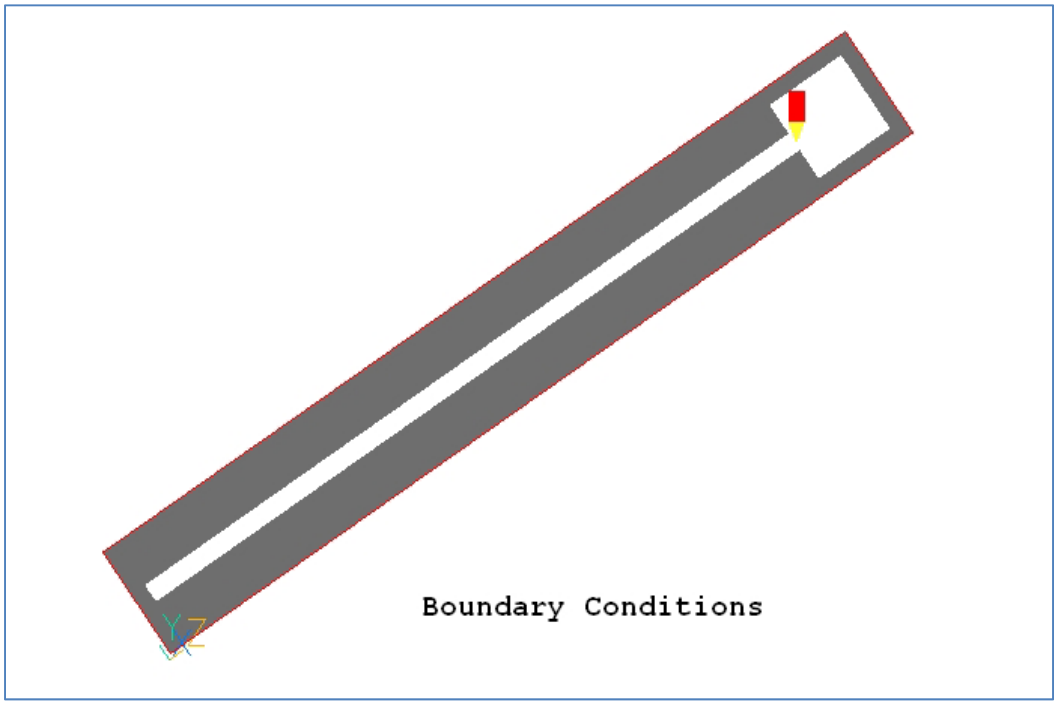

Figure 3-1: Diagram of Computational Domain

Figure 3-1 shows the computational domain used for the numerical study. The Z direction is the long direction, the Y direction is the short direction and the X direction is not represented.

The study was performed in two dimensions. The domain was bounded in the X planes via symmetry and the Y and Z planes with plates at 14 °C to simulate the ambient temperature. Gravity sources were broken down into Y and Z components based on the 40° tilt.

The grey blockages of Figure 3-1 are simulated as polyurethane insulation similar to that used in the experiment. Where the blockages are thinner, the thickness is 3.8 cm representing the thickness of the insulation used around the fishbowl. Where these blockages are thicker, the thickness is 10cm which is used as an approximation to the U value of an evacuated tube. This is a reasonable approximation as the

thermal conductivity of polyurethane is 0.03 W/m-K, which at 10 cm thick matches the U- value of a well-constructed evacuated tube. All of the interior surfaces were modeled as no-slip with a roughness equal to that of borosilicate glass. Solar radiation is represented by a plate on the top of the long fluid domain with a heat flux of 910 W/m^2 which takes into account the 1000 W/m^2 and an optical efficiency of 0.91.

3.1.4 Grid Independence

A grid independence study was conducted. It was determined that results were reasonably grid independent with 56 cells in the Y direction and 404 cells in the Z direction. This is a good compromise between numerical accuracy and computing time.

3.1.5 Results

3.1.5.1 Temperature Contours

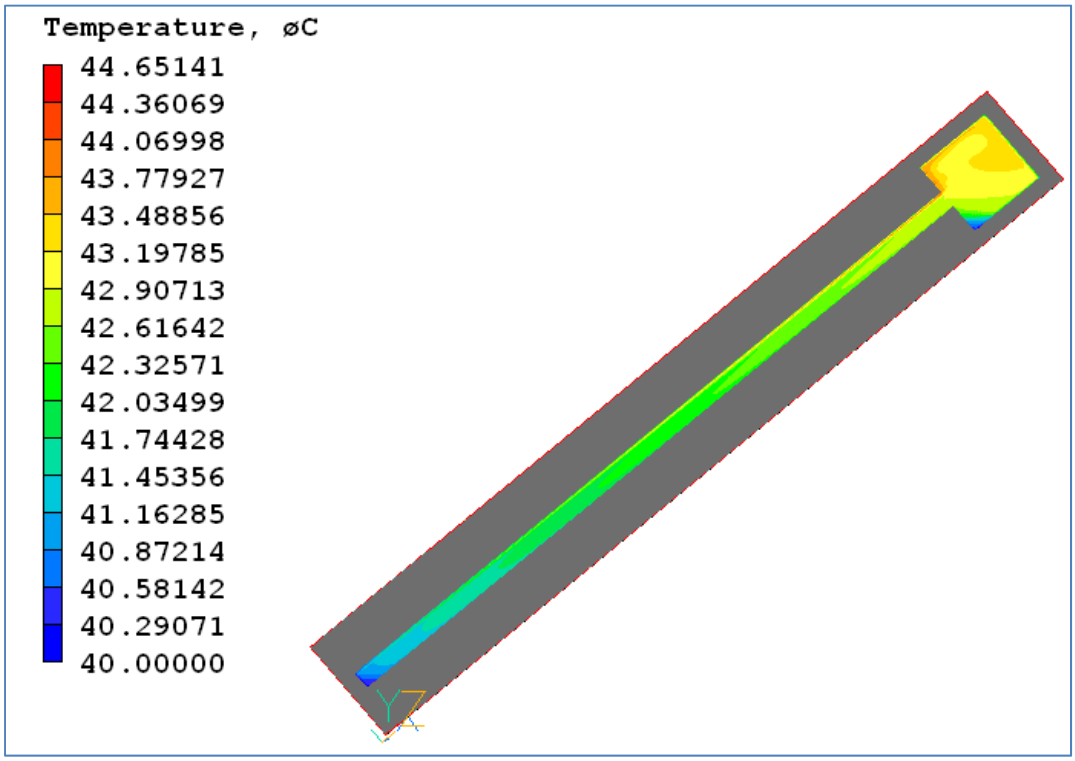

Figure 3-2: Temperature Contours along the length of the tube

Figure 3-2 stands to answer the first objective question posed in the introduction. It can be seen in the figure that the temperature contours are fairly consistent from the top of the tube to the bottom of the tube in the "Y" direction with gradients at approximately 1.5°C at the bottom to slightly more than 2 °C near the mouth of the tube. It can also be seen that the temperature has a consistent gradient in the "Z" direction, increasing from the bottom to the top. Once the hot fluid reaches the tube opening it follows along the edge of the tank to the uppermost corner where it starts to cool and then recycles back to the bottom of the tube.

3.1.5.2 Velocity Comparisons to Budihardjo

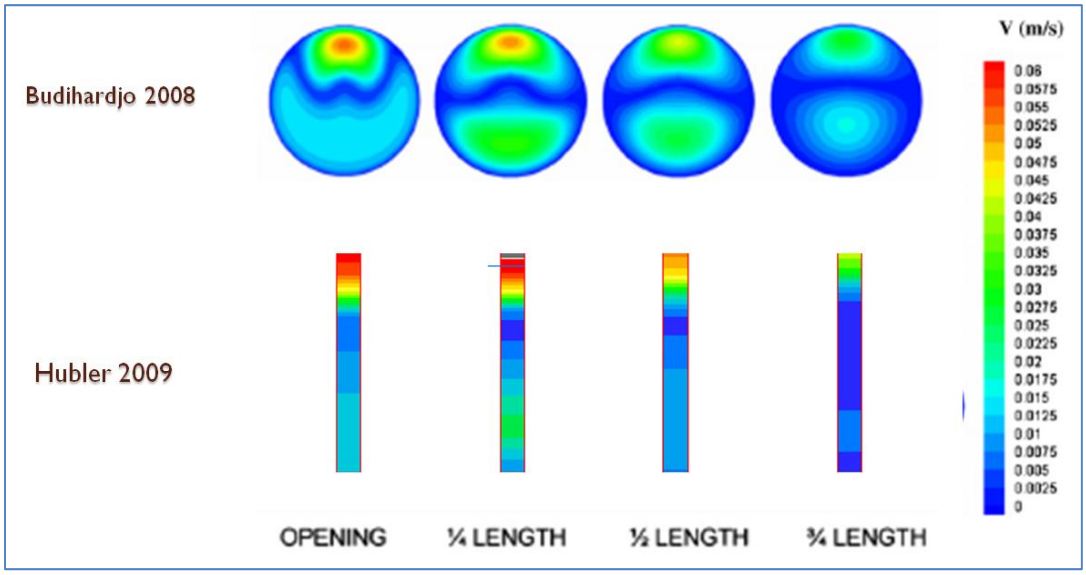

Figure 3-3: Comparison of Velocity Profiles to Budihardjo, (upper images from Budihardjo 2008)

Figure 3-3 above shows a comparison of this study's velocity profiles in the axial direction of the tube to those reported by Budihardjo. The different profiles are taken at different points along the length of the tube from the tube opening to ¼ of the way from the bottom of the tube. It can be seen that the two profiles, for the most part, match up. Differences can be attributed mostly to differences in grid size and the two dimensional nature of the case considered in this paper.

3.1.5.3 Transient Heat-Up Comparison

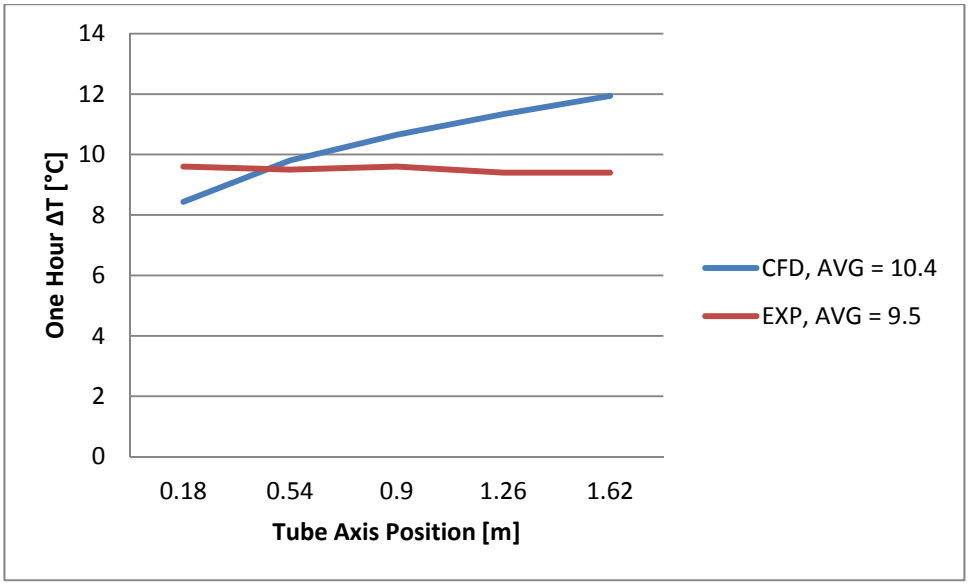

Figure 3-4: Comparison of CFD prediction of 1 hour heat up vs measured

Figure 3-4 shows the CFD modeled heat up compared to the measured heat up for a one hour period starting at an initial temperature of 76.6 °C. The blue line represents the CFD model while the red line represents the experimental values. The position is listed on the x axis of the graph. It can be seen that overall, the temperature change was very even for the experimental measurements ending up with an average heat up of 9.5 °C. For the modeled heat-up, it can be seen that points nearer the tube opening heat up more than points at the bottom of the tube. The average overall heat up rate for the model is 10.4 °C.

3.1.6 Conclusions

This study set out to answer three objective questions:

1. Is a single thermocouple placed at the axis of the tube sufficient to measure accurately the temperature inside the tube?
2. Do the modeled axial velocity profiles match those reported by Budihardjo (2008)?

3. Does a transient, one hour heat up simulation match the experimental measured temperature rise?

To start, it appears that the temperature profile in the radial direction of the tube is fairly even, i.e. there is no significant temperature change in the radial direction of the tube. Temperature does appear to increase from the bottom of the tube to the tube opening but these changes are fairly gradual. It appears therefore that a single thermocouple mounted at the axis of the tube is sufficient to accurately measure the tubular temperature for that section.

When compared to the velocity profiles reported by Budihardjo, the axial velocity profiles determined in this study match up well. It should also be noted that in all of the locations depicted in Figure 3-3, the velocities near the axis of the tube are near zero. This shows that the placement of the thermocouple and polycarbonate rod at the center of the tube will not adversely affect the natural flow patterns inside the tube.

Finally, when a transient numerical simulation of a one hour temperature increase was performed, it matched the measured temperature increase very well. The modeled increase was 10.4 °C and the measured increase was 9.5 °C

4 DATA ANALYSIS AND METHODOLOGY

4.1 Mass and Volume Data from Experiment

Mass and volume data from solution samples taken before and after boiling were used to determine the mass fraction of the solution. Any increases in mass fraction from initial concentrations to final concentrations are evidence of regeneration of the desiccant. Section 4.1 explains the method from which mass and volume can be converted to a mass fraction and compares the calculated mass fraction from the initial solution to the final solution.

4.1.1 Initial Solution Data

Section 2.3.1 outlines the method in which samples were collected and tested for the initial solution. Table 4-1 shows the mass, volume and temperature as well as the calculated density for the five samples taken for the 10% nominal mass fraction solution

Table 4-1: Data collected for 10% Nominal Solution

Sample Number	Mass [g]	Volume [ml]	Temperature [°C]	Density [kg/m3]
1	543.5	500	24	1087
2	543.5	500	24	1087
3	544.5	500	24	1089
4	543.5	500	24	1087
5	543.5	500	24	1087

Mass, volume and temperature are directly measured. Density is calculated by simply dividing mass by volume. The density and temperature are related to the mass fraction of the solution through the correlation proposed by Conde.

$$\rho_{sol}(T,\xi) = \rho_{H_2O}(T)\left(1 + 0.836014\left(\frac{\xi}{1-\xi}\right) - 0.436300\left(\frac{\xi}{1-\xi}\right)^2 + 0.10564\left(\frac{\xi}{1-\xi}\right)^3\right) \quad (4\text{-}1)$$

Where ξ is the solution mass fraction, ρ_{H_2O} is the density, in kg/m^2 of pure water at the corresponding temperature given by,

$$\rho_{H_2O}(\tau) = \rho_{c,H_2O}\left(1 + B_0\tau^{1/3} + B_1\tau^{2/3} + B_2\tau^{5/3} + B_3\tau^{16/3} + B_4\tau^{43/3} + B_5\tau^{110/3}\right) \quad (4\text{-}2)$$

with τ defined by equation 4-3 below.

$$\tau = 1 - \frac{T}{T_{c,H_2O}} \quad (4\text{-}3)$$

In equation 4-3, T_{c,H_2O} is the critical temperature of water, (647.1 K) and T is the temperature of the solution in K. The coefficients B_i are given in Table 4-2 below.

Table 4-2: Coefficients for Water Density Equation

i	Bi
0	1.993772
1	1.098521
2	-0.50945
3	-1.76191
4	-44.9005
5	-723692

Equation 4-1 is set up to solve for density given a mass fraction. In this case, mass fraction is desired and density is known. Because of the complexity of Equation 4-1, it cannot be re-arranged explicitly. Therefore, mass fraction as a function of solution density was solved numerically. This method was used to determine both the initial and final mass fraction of all of the samples of solution.

4.1.2 Final Solution Data

Once the solution was boiled, the final mass fractions were calculated using the same method as the initial mass fractions. Because the final solutions were analyzed directly after boiling, the solution temperatures were much more than the initial samples and temperature became more of a factor in the calculations.

4.2 Pressure Analysis

As the solution inside the tube heated up in the sun, the thermocouple at the bottom of the tube maintained a slightly lower temperature than the thermocouple at the top of the tube. This stands to reason as natural convection and buoyancy forces will create a small amount of stratification in the tube as it is heated by the sun's radiation. As the solution neared the boiling regime the thermocouples measured a temperature inversion where the thermocouple at the bottom of the tube had the highest temperature and the thermocouple at the top of the tube had the lowest temperature. Figure 4-1 depicts this temperature inversion.

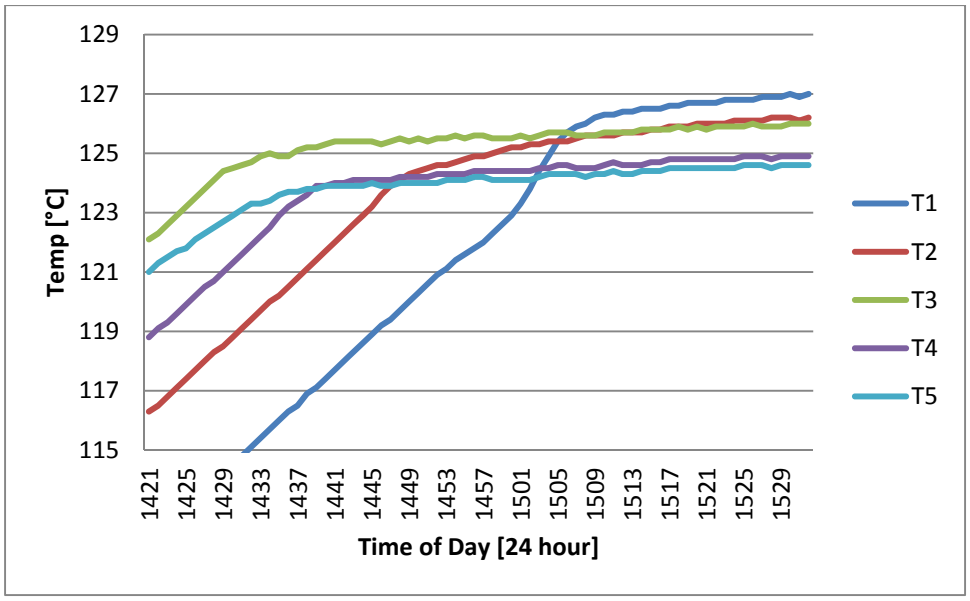

Figure 4-1: Temperature as a Function of Time for the Five Thermocouples Inserted in the Evacuated Tube for a 50% Nominal Solution

Initially it was feared that this temperature inversion could be caused by an increased mass fraction at the bottom of the tube and decreased mass fraction at the top of the tube. This was feared because the density function of the calcium chloride solution is much more dependent on solution mass fraction than on solution temperature and the denser, more concentrated solution could be collecting at the bottom of the tube. This stratification of concentration could potentially render the apparatus ineffective at regenerating the solution as the concentrated solution would be permanently stuck in the bottom of the tube. In fact, this inversion can instead be completely attributed to a difference in static pressure at the thermocouples. This static pressure difference is created by differences in depth of the thermocouples in the solution and defined by, $P = \rho g h$, where ρ is defined by Equation 4-1, h is the depth of the thermocouple in the solution and g is the acceleration due to gravity. For clarity, Figure 4-2 depicts this depth of solution represented in the figure as "h" which is defined as the vertical distance between the surface of the solution and the thermocouple.

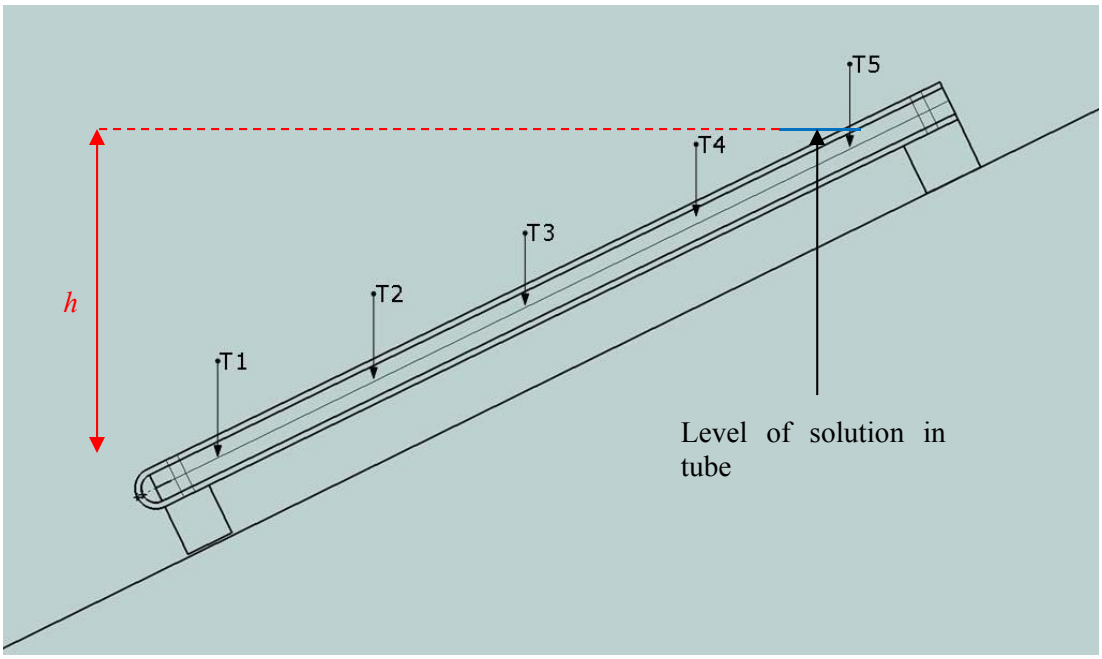

Figure 4-2: Diagram of Water Column for Thermocouples

4.2.1 Calculating Pressure in Tube

The effects of height, pressure, and temperature can be examined by considering the formation of a vapor bubble during boiling. When a bubble forms, saturated water vapor at the local pressure separates from the solution. The vapor inside the bubble is at the same pressure as the vapor pressure of the solution. This solution vapor pressure is a function of the temperature of the solution as well as the mass fraction of the solution. But, since during boiling bubbles are forming that are in equilibrium with the local pressure, the solution vapor pressure is also equal to the total pressure at each thermocouple. This local pressure is the sum of atmospheric and solution static pressure from the product of $\rho g h$ described above. It is convenient to characterize the solution vapor pressure as a fraction of vapor pressure relative to the saturated vapor pressure of pure water at the same temperature. Conde defines this reduced pressure as,

$$\pi = \frac{P_{sol}(\xi, T)}{P_{H_2O,Sat}(T)}$$

$$= \left\{1 - \left[1 + \left(\frac{\xi}{0.478}\right)^{-5.20}\right] - 0.018e^{-\frac{(\xi-0.1)^2}{0.005}}\right\}\left\{\left[2 - \left[1 + \left(\frac{\xi}{0.31}\right)^{3.698}\right]^{0.60}\right]\right. \quad (4\text{-}4)$$

$$\left. + \left[\left[1 + \left(\frac{\xi}{0.231}\right)^{4.584}\right]^{0.49} - 1\right]\theta\right\}$$

where $P_{\mathrm{H_2O}}(T)$ is the vapor pressure of pure water. Saturated vapor pressure as a function of temperature for pure water is a well studied quantity and can be found in nearly every fluid mechanics textbook. There are also empirical formulations for vapor pressure as a function of temperature. One of the most widely recognized formulations of saturated vapor pressure as a function of temperature is provided by Keenan and Keyes (1969),

$$P_{H_2O,Sat} = 22105649.25e^{\frac{-27405.526+97.5413T-0.146244T^2+0.00012558T^3-0.000000048502T^4}{4.34903T-0.0039381T^2}} \quad (4\text{-}5)$$

where T is the temperature of water in K and $P_{H_2O,Sat}$ is the saturated pressure of the water in Pascals. Dividing the sum of atmospheric and solution depth pressure by the result of equation 4-5 gives a reduced pressure for each thermocouple as a function of time. Equation 4-4 can then be used to calculate the mass fraction of the solution at each thermocouple as a function of time for each time step during which boiling occurs.

In order to predict, as expected, that the mass fraction of the solution increases with time, it is necessary to account for the evaporation of water. When water evaporates, it decreases the height of the solution/air interface, h, which in turn decreases the solution saturation pressure. A decreased solution saturation pressure corresponds with a higher mass fraction. To determine the amount by which h is decreased, the volume of water evaporated from the following solar analysis is used. Using this volume, the following relation can be used to determine the height of water evaporated,

$$dh = \frac{dV}{A}\sin\Theta \qquad (4\text{-}6)$$

In equation 4-6, A is the cross sectional interior area of the tube and Θ is the angle of the tube. . The results of equation 4-6 can be subtracted from the initial height of the solution column above each thermocouple. As explained above this will reduce the overall pressure at each point which in turn will correspond to increasing mass fractions as a function of time.

In similar fashion to equation 4-1 equation 4-4 gives a relation for the reduced pressure of the solution as a function of solution mass fraction. A plot of reduced pressure vs. solution mass fraction was created with the reduced pressure as the independent variable. A more simple polynomial regression was used to relate solution mass fraction as a dependent variable to reduced pressure. Figure 4-1 shows this regression.

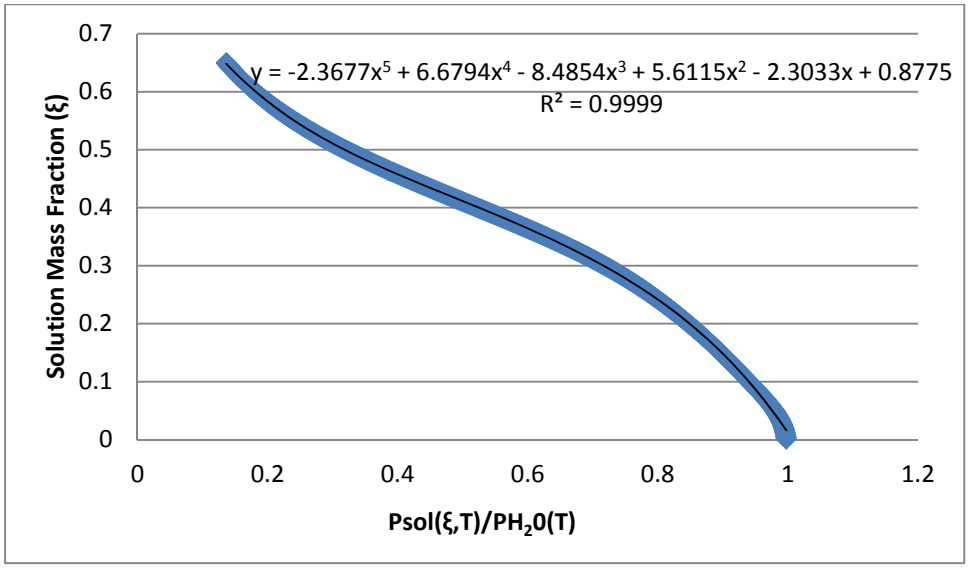

Figure 4-3: Regression for Mass Fraction as a Function of Reduced Solution Pressure

Equation 4-7 is the equation of the polynomial displayed in Figure 4-3

$$\xi = -2.367\pi^5 + 6.679\pi^4 - 8.485\pi^3 + 5.611 - 2.303\pi - 0.877 \qquad (4\text{-}7)$$

with π being a variable coined by Conde to represent the reduced pressure of the solution as given by equation 4-4.

In reality, the reduced pressure of the solution is both a function of solution temperature AND mass fraction. Therefore, the relation provided by equation 4-7 is only valid for the boiling temperature of a 10% nominal mass fraction solution and this regression has to be repeated for the other nominal mass fraction solutions. As the mass fraction increases during boiling, the boiling temperature does not increase significantly. Therefore, the relation provided by equation 4-7 is valid for the entire time the solution is boiling.

When the density at each thermocouple is examined, it can be seen that there is very little stratification due to mass fraction indicating that the temperature inversion is indeed caused solely by the increase in pressure due to the solution above each thermocouple. The results of this analysis will be further examined in Chapter 6.

4.3 Solar Radiation Analysis

This section outlines the method used to predict collector performance based on measured solar radiation and position. First the Perez sky model is introduced and explained as it is the sky model used for this analysis. Next a definition of solar angles and the equations used to calculate them are presented for both arbitrarily positioned flat plates and tubular collectors. These angles are then used with the radiation terms from the Perez sky model to determine radiation incident on flat plate and tubular collectors. The method for determining absorbed radiation based on this incident radiation is next presented. Absorbed radiation is then used to calculate the amount of water boiled based on solution properties.

4.3.1 Basic Measured Solar Radiation Values

Solar radiation data were taken from the National Renewable Energy Lab (NREL) Solar Radiation Research Laboratory (SRRL) Baseline Measurement System (BMS). Figure 4-4 shows the location of the SRRL relative to the location at which the experimental apparatus was located. It can be seen in the figure that the solar radiation measurements were taken less than 300 meters from where the experiment took place.

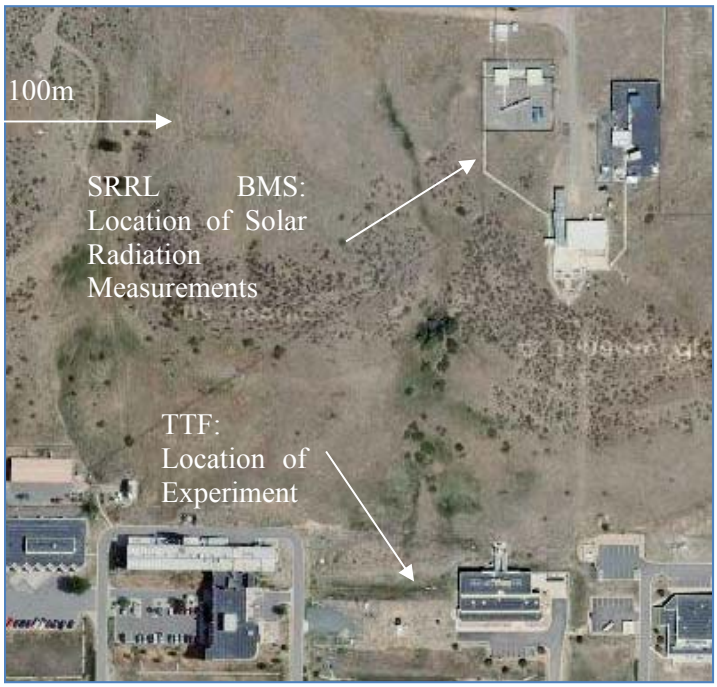

Figure 4-4: Location of Experimental Apparatus in Relation to Location of Solar Radiation Measurement Devices

The irradiance values used in this analysis are direct normal, horizontal diffuse, and global horizontal. Direct normal radiation is measured by a Kipp & Zonen pyrheliometer. Global horizontal is measured with a Kipp & Zonen CM-22 pyranometer with calibration factor traceable to the World Radiometric Reference. Diffuse irradiance is measured by an Eppley 8-48 Black & White Pyranometer mounted under the shading ball of a Sci-Tec tracker. These instruments provide irradiance as W/m^2 and

are published with one minute resolution by the SRRL. For subsequent analysis this one-minute solar data is averaged over a five minute period to reduce data noise.

4.3.2 Solar Angles

Solar azimuth (γ) and zenith (θ_z) are the basic angles that describe solar position as the sun tracks across the sky. Azimuth angle is defined as the angle created by a line projected on the horizontal between the sun and the point of reference and a line going from the point of reference due south. Zenith angle is defined as the angle between a vertical line and a line from the point of reference and the sun. These two angles are instrumental in calculating all other incidence angles, both on flat plates and evacuated tubes. For this analysis the angles are reported by the NREL SRRL and are both calculated using the solar position algorithm developed by Reda and Andreas (2004). This algorithm predicts solar position as a function of time with an uncertainty of +/- 0.0003 degrees.

4.3.3 Incidence Angle on a Sloped Surface

Incidence angle on a sloped surface (θ'), defined as the angle between the sun and the normal to the sloped plane, can be calculated by using basic trigonometry in equation 4-8 below.

$$\theta' = \cos^{-1}(\cos\theta_z \cos\beta_s + \sin\theta_z \sin\beta_s \cos(\gamma - \gamma_s')) \qquad (4\text{-}8)$$

Equation 4-8 uses the previously defined solar position zenith and azimuth angles. In addition, equation 4-8 uses β defined as the angle between the sloped surface and the horizontal and γ' which is the angle between the projection of the normal on the horizontal and due south. This angle is used for determining the beam component of radiation incident on the roof behind the tube which will be further explained in section 4.3.5.5 below.

4.3.4 Incidence Angle on a Tubular Collector

Perez (1995) proposed that cylindrical evacuated tubes act as single-axis tracking flat plate collectors with a tracking axis parallel to the axis of the tube. Because of this, solar incidence on the tube will always be in the longitudinal direction in the plane containing the sun and the axis of the tube. Figure 4-5 shows a depiction of this angle. The angle Z in the figure is the solar zenith angle.

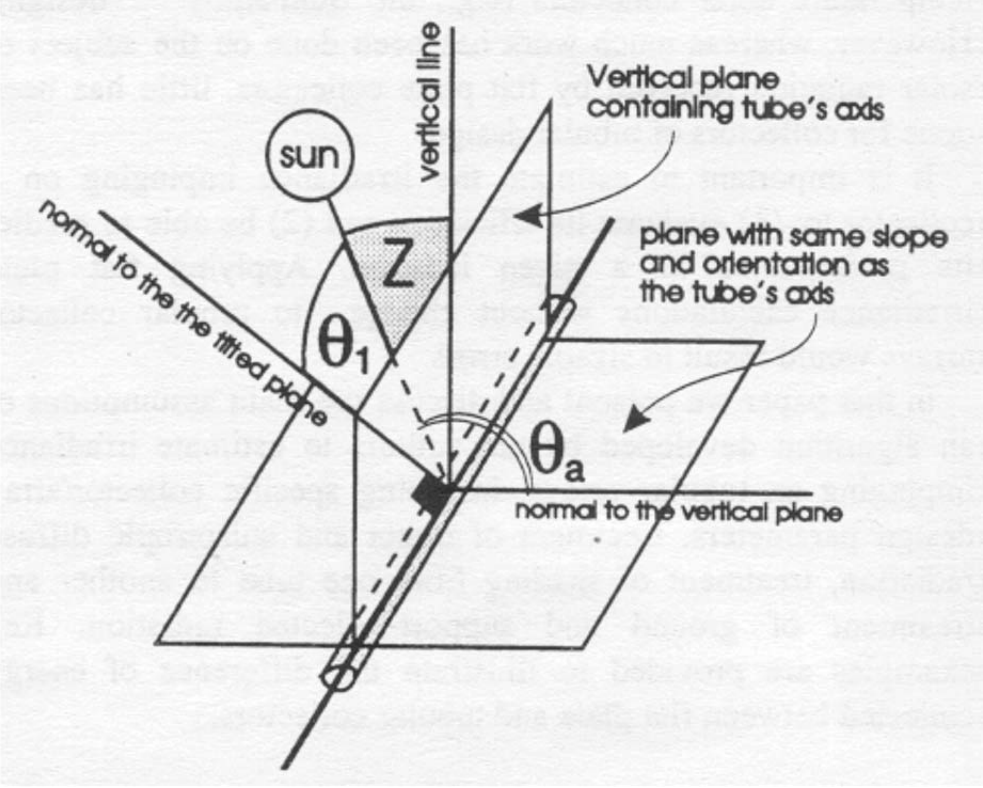

Figure 4-5: Depiction of the Incidence Angle of the Sun on a Tubular Collector from (Perez 1995)

This incidence angle, θ, is defined by,

$$\theta = \cos^{-1}\left(\frac{\cos\theta_1}{\cos\alpha}\right) \tag{4-9}$$

where θ_1 is the incidence angle on a sloped surface with the same slope and orientation as the axis of the tube given by the equation

$$\theta_1 = \cos^{-1}(\cos\theta_z \cos\beta_t + \sin\theta_z \sin\beta_t \cos(\gamma - \gamma_t')) \quad (4\text{-}10)$$

Equation 4-10 is essentially the same as equation 4-8. The difference being β_t is the angle between the axis of the tube and horizontal and γ_t' is the azimuth of the tube. α, which can be described as the projection of the sun on a plane perpendicular to the axis of the tube is defined as,

$$\alpha = ATAN2[\cos\theta_1, \cos\theta_a] \quad (4\text{-}11)$$

The function ATAN2 returns the arc tangent angle based on its Cartesian coordinates [x,y]. θ_a is the incidence angle on a surface with $\gamma_s = \gamma_t' - 90°$ and $\beta = 90°$.

4.3.5 Perez Sky Model

To determine the radiation incident on the tube, the Perez sky model (Perez 1990) is used. This model takes into account that the sky is brighter around the sun and near the horizon instead of treating the sky as isotropic. The model effectively breaks the solar radiation into six parts. The first is the direct irradiance coming from the disk of the sun. The second, called circumsolar diffuse, is the diffuse light coming from the sky circumscribing the sun. The third is the diffuse light coming from directly above the horizon. The horizon is slightly brighter than the rest of the diffuse sky due to the reflection from the ground. The fourth portion of radiation from the sky in the Perez model is the diffuse radiation from the remainder of the sky, this portion is treated as isotropic. The fifth portion of radiation is the reflected diffuse radiation from the ground. The sixth portion of radiation is the diffuse radiation reflected from the roof behind the tube. Perez relates the diffuse portions of sky radiation by factors such as cloud cover and air clarity. In another paper Perez (1995) expands upon his sky model by using the components of sky radiation to calculate the incident radiation on evacuated tube. This method, described in detail

immediately below, is how incident radiation was calculated from the available solar data from NREL in this experiment.

4.3.5.1 Direct Irradiance

With the incidence angle on the tube, θ, calculated, direct radiation incident on the tube, B_c, is simply,

$$B_c = Bcos\theta \tag{4-12}$$

Where B the measured direct normal irradiance from the, from the Kipp & Zonen pyrheliometer.

4.3.5.2 Circumsolar Diffuse

Circumsolar diffuse radiation is the disc of radiation near the sun that tends to be brighter than the other regions of the sky. Since this radiation is circumsolar it is incident on the tube at the same angle θ as the direct radiation. Perez defines this circumsolar radiation by,

$$Dc_{circumsolar} = \frac{Dh * f_1 * \cos\theta}{Max(0.087, \cos\theta_z)} \tag{4-13}$$

Where Dh is the horizontal diffuse radiation as measured by the Eppley Black 8-48 & White Pyranometer and f_1 is the circumsolar enhancement parameter from Perez et al (1990). The function "Max" simply returns the maximum of two values.

4.3.5.3 Isotropic Diffuse

Again, from Perez, the isotropic diffuse radiation incident on the tube is given by,

$$Dc_{iso} = Dh\left[\frac{(1-f_1)(1+\cos\beta_t)}{2} + f_2 \sin\beta_t\right] * \frac{\pi}{2} \tag{4-14}$$

Where f_2 is the horizon enhancement coefficient from Perez et al (1990) The $\pi/2$ factor comes about when one integrates the diffuse radiation over the dome of the sky with the curved surface of the tube.

4.3.5.4 Ground Reflected

Ground reflected radiation is a function of the global horizontal radiation, Gh, measured by the Kipp & Zonen CM-22 pyranometer and is given by:

$$Rc = Gh * a * (1 - \cos\beta_t) * \frac{\pi}{4} \tag{4-15}$$

Where a is the albedo also reported by NREL SRRL. The $\pi/4$ factor at the end of the equation comes about for similar reasons to the $\pi/2$ factor at the end of equation 4-14.

4.3.5.5 Roof Reflected

Roof reflected radiation is the total incident radiation on the tilted surface behind the tube multiplied by the albedo of the surface. The total incident radiation on the roof is calculated same components as incident radiation on a tube except that the incidence angle of direct radiation is the incidence on a tilted surface instead of the incidence angle on a tube. Additionally, the $\pi/2$ and $\pi/4$ factors for isotropic diffuse and ground reflected radiation respectively are not present as the roof is a flat surface. Combining the components from sections 4.3.5.1 to 4.3.5.4 gives a total incident radiation on a combined surface as:

$$G_R = Bcos\theta' + \left(\frac{Dh * f_1 * \cos\theta'}{Max(0.087, \cos\theta_z)}\right) + \left(Dh\left[\frac{(1-f_1)(1+\cos\beta_s)}{2} + f_2 \sin\beta_s\right]\right) + (Gh * a * (1 - \cos\beta_s)) \tag{4-16}$$

Using G_R from equation 4-16 the reflected radiation from the roof incident on the tube is,

$$RRc = G_R * a_R * \frac{\pi}{4} \tag{4-17}$$

Where a_R is the albedo of the roof, and $\frac{\pi}{4}$ is the cylindrical tube factor.

4.3.5.6 Total Radiation Incident on a Tubular Collector

Taking all of the components described above, the total radiation incident on a tubular collector is:

$$G_t = Bcos\theta + \left(\frac{Dh * f_1 * \cos\theta}{Max(0.087, \cos\theta_z)}\right) + \left(Dh\left[\frac{(1-f_1)(1+\cos\beta_t)}{2} + f_2 \sin\beta_t\right]\right) + (Gh * a * (1-\cos\beta_t)) + \left(G_R * a_R * \frac{\pi}{4}\right) \tag{4-18}$$

4.3.6 Solar Thermal Efficiency

4.3.6.1 Approach

Solar collector efficiencies are found by taking the amount of useful energy produced by a collector and dividing that energy by the solar energy incident on the collector. In typical solar collectors, the useful energy is realized as a sensible heating of a fluid. In typical efficiency determinations, fluid is pumped through a collector at a known flow rate and the change in temperature is used to determine the heat gained by the fluid and ultimately the thermal efficiency of the collector.

Of paramount interest in this experiment is the amount of water evaporated from a solution during boiling. The useful energy produced by the solar collector is the amount of energy used to evaporate water. Proper measurement of useful energy would require measurement of water evaporation rate. Since the experimental apparatus did not allow direct measurement of the amount of water being evaporated in real-time, the following method was used to determine collector efficiency: First, useful

energy was measured with the thermocouples during the period of time in which the solution inside the tube was heating up prior to boiling. This temperature change in conjunction with the heat capacity of the tube components and the fluid could be used to determine useful energy. This analysis, as previously described, is conducted on a five-minute time step in phase with the solar radiation data. Second, this useful energy is divided by the corresponding incident radiation to determine efficiency. Third, this efficiency is correlated to the incident radiation, interior tube temperature and ambient temperature over a range of values to determine a characteristic efficiency equation of the tube. Lastly, this characteristic equation is used in conjunction with measured interior temperature, ambient temperature and incident radiation to determine useful energy during boiling. This useful energy is used in section 4.3.7 to determine the amount of water boiled from the tube. This entire procedure is described in further detail below.

4.3.6.2 Q_{useful} During Warmup

To determine how much radiation is actually usefully absorbed by the tube, temperature data from the thermocouples is used. When the tube is heating up, the volumetric average temperature of the five thermocouples is taken to give a representative average internal temperature of the tube (T_i). The difference in this average temperature over the five minute measurement time step multiplied by the heat capacity of the solution and tube gives a useful energy described further by the following equation.

$$Q_{useful} = \left(T_{i,final} - T_{i,initial}\right)\left(m_{sol}c_{p,sol} + C_t\right) \qquad (4\text{-}19)$$

Where C_t is the heat capacity of the interior glass tube and rubber stopper, m_{sol} is the mass of the solution in the tube and $c_{p,sol}$ is the temperature and mass fraction dependant specific heat of the solution given by Conde as,

$$
\begin{aligned}
&c_{p,sol}(T,\xi) \\
&\quad = c_{p,H_2O}(\theta(T))\big(1 \\
&\quad - (1.63799\xi - 1.69002\xi^2 + 1.05124\xi^3)(58.5225\theta^{0.02} - 105.6343\theta^{0.04} \\
&\quad + 47.7948\theta^{0.06})\big)
\end{aligned} \tag{4-20}
$$

Where $c_{p,H_2O}(T)$ is the temperature dependant specific heat of pure water given by,

$$
\begin{aligned}
&c_{p,H_2O}(\theta(T)) \\
&\quad = 88.7691 - 120.1958\theta^{0.02} - 16.9264\theta^{0.04} + 52.4654\theta^{0.06} + 0.10826\theta^{1.8} \\
&\quad + 0.46988\theta^{8}
\end{aligned} \tag{4-21}
$$

and θ defined by,

$$
\theta \stackrel{\text{def}}{=} \frac{T}{288} - 1 \tag{4-22}
$$

Where T has units of Kelvins and the 288 factor is a regression factor determined by Conde (2004).

4.3.6.3 Tube Efficiency

As mentioned previously the instantaneous efficiency, or more practically in this case the efficiency of each data time step can be given by,

$$
\eta = \frac{Q_{useful}}{300AG_t} \tag{4-23}
$$

Q_{useful} is an energy term with the units of Joules. Incident radiation on the tube given by equation 4-18 is still in the units of W/m^2. G_t is multiplied by the collector area and 300, or the number of seconds in a five-minute time step, to keep the units consistent between the numerator and denominator of the equation.

4.3.6.4 Developing Efficiency Curves

In addition to the efficiency equation above, Q_{useful} is also a function of the energy balance of the tube. More specifically, it is solar energy absorbed by the tube less the energy dissipated through thermal losses. This function can be given by the classic solar collector energy balance equation

$$Q_{useful} = AF_R[S - U_L(T_i - T_a)] \quad (4\text{-}24)$$

Where A is defined for this analysis as the area of the absorber, F_R is the heat removal factor of the collector that is related to a heat exchanger effectiveness, S is the solar radiation absorbed by the collector per unit area, U_L is the overall heat transfer coefficient of the tube, T_i is the average internal fluid temperature and T_a is the ambient air temperature outside of the tube.

The absorbed radiation, S, can be related to the total incident radiation, G_t, by the introduction of the transmittance-absorptance product, or $(\tau\alpha)$, which is a combined property of the outer glass tube and the surface of the inner tube. It should not be thought of as a product of two separate properties, but rather a single property of a collector. The collector heat balance equation including these new terms is shown below.

$$Q_{useful} = AF_R[G_t(\tau\alpha)_e - U_L(T_i - T_a)] \quad (4\text{-}25)$$

The subscript, *e*, in the above equation refers to the effective transmittance absorptance product. Research has shown that the $(\tau\alpha)$ product is not constant, but varies with the incidence angle of the radiation on the collector. ASHRAE Standard 93 (ASHRAE 2003) for testing and determining the efficiency of flat plate collectors, provides for a factor called the incidence angle modifier, referred to as K to adjust the $(\tau\alpha)$ product based on the incidence angle of the radiation. ASHRAE Standard 93 gives an expression for K as a function of the incidence angle as,

$$K = 1 - b_0\left(\frac{1}{cos\theta} - 1\right) \tag{4-26}$$

Where b_0 is the mean incidence angle modifier coefficient and is a characteristic parameter of the collector. Theunissen and Beckman (Theunissen 1985), determined the mean incidence angle modifier coefficient for a tubular collector with a diffuse reflector to be -0.15.

With the incidence angle modifier introduced, the heat balance equation can be updated as,

$$Q_{useful} = AF_R[KG_t(\tau\alpha)_N - U_L(T_i - T_a)] \tag{4-27}$$

With the incidence angle modifier introduced, it becomes important to use $(\tau\alpha)_N$ in the collector heat balance equation. $(\tau\alpha)_N$ is the transmittance-absorptance product of the collector at normal incidence. Theunissen and Beckman have determined this to be 0.874.

Using the temperature and solar data, efficiencies for every five minute time step during the heat up of the solution can be calculated. Efficiencies by themselves are not useful however. ASHRAE Standard 93, correlates the efficiency of the collector to the term,

$$\frac{T_i - T_a}{G_t} \tag{4-28}$$

All of the terms of equation 4-28 have been previously defined. If equation 4-28 is calculated for each five minute time step and then plotted as the independent variable against efficiency, the result is a characteristic curve that will predict tubular collector performance for all circumstances. This characteristic curve takes the form

$$\eta = m\left(\frac{T_i - T_a}{G_t}\right) + \eta_{max} \tag{4-29}$$

Where m is the slope of the characteristic curve and η_{max} is the theoretical maximum efficiency of the collector that occurs when the temperature inside the collector is equal to the ambient temperature. This situation means that effectively there are no thermal losses and the efficiency is based solely on the optical efficiency of the collector. In other words, how much of the radiation that is incident on the tube gets absorbed into the fluid inside as opposed to reflecting off of the tube.

Since Q_{useful} calculated by equation 4-19 is only valid while the tube is heating up, the characteristic performance curve must be used to predict tube performance when the solution is boiling. By knowing the efficiency of the tube at any time during boiling, as well as the incident radiation on the tube, once can calculate a new, Q_{useful} and use it to predict the amount of water evaporated during boiling.

4.3.7 Evaporated Water

The parameters, m and η_{max} from equation 4-29 are determined during the heat up phase of the experiment and are characteristic of the tube, meaning that they should be the same for each individual test performed, as discussed further in Section 6. Given that all of the other independent variables of equation 4-29 are known, equation 4-29 can be used to calculated a different Q_{useful} given by,

$$Q_{useful,boiling} = m_{H_2O}\left(h_{fg} + h_s\right) \tag{4-30}$$

Where m_{H_2O} is the amount of water boiled, h_{fg} is the heat of vaporization of water and h_s is the differential enthalpy of dilution, or in other words, the amount of energy needed to bring water out of solution with the calcium chloride before it is evaporated. Conde supplies a relation for this as a function of the solution temperature and mass fraction given by,

$$h_s = [3011.974\theta - 955.690]\left[1 + \left[\frac{\left(\frac{\xi}{0.8-\xi}\right)}{0.855}\right]^{-1.969}\right]^{-2.265} \quad (4\text{-}31)$$

Both θ and ξ have been previously defined as a normalized temperature (equation 4-22) and solution mass fraction, respectively.

Knowing h_s, equation 4-30 can be rearranged to give,

$$m_{H_2O} = \frac{Q_{useful,boiling}}{(h_{fg} + h_s)} \quad (4\text{-}32)$$

Equation 4-32 gives the mass of water evaporated as a function of $Q_{useful,boiling}$ and the sum of the heat of vaporization of water and the differential enthalpy of dilution. This mass of water is the prediction of water evaporated for one time step during boiling. When the sum of all boiling time steps is taken, this is the total mass of water evaporated during a test procedure as predicted by the model introduced in this thesis. This result should be compared to the directly measured amount of water boiled as explained in section 4.1. This comparison, and other discussion of results is found in Chapter 6

5 UNCERTAINTY ANALYSIS

When collecting data, it is important to conduct an uncertainty analysis to determine the validity of the data. Uncertainty gives a range of measured values within which the true value of a parameter is likely to be. In this experiment, data was collected in both single measurements and multiple sample measurements of a single value. Each way of collecting data requires different uncertainty analysis techniques. These uncertainty analysis techniques are further discussed in the following sections divided by the type of data for which statistical uncertainty is desired. Regardless of the technique used to determine uncertainty, a confidence interval of 95% was used for all data.

5.1 General Methodology

Throughout this analysis, uncertainty is calculated using the following overall methodology, outlined by ASME (1998) and recommended by Wheeler and Ganji (2004):

5.1.1 List all Elemental Error Sources

All the sources of elemental error are cataloged, including errors due todevice resolution, calibration, data reduction and uncertainty due to measurement methods. It is helpful to list these sources of error in tabular format. For the purpose of this analysis, the elemental error sources affecting a certain parameter will be listed in a separate table for each sub-section.

5.1.2 Estimate the Elemental Errors

The magnitude of the errors for all the listed elemental error sources must be evaluated. These estimates generally include the variance or standard deviation of error distributions and any uncorrected bias errors.

5.1.3 Calculate the Random Uncertainty of Each Measured Variable

Uncertainty from random variation in repeated experiments is calculated. As with the other steps in this process it is helpful to show this uncertainty as a standard deviation about a calculated mean value The mean value $\bar{x}$, of the data set is the simple arithmetic mean of the data and is given by,

$$\bar{x} = \frac{1}{N}\sum_{i=1}^{N} x_i \tag{5-1}$$

where N is the number of measurements in the data set and x_i is the value for each of the measurements.

Measured data is expected to be randomly distributed about the mean value according to the normal distribution. The difference between any value x_i and the mean value is categorized by the sample standard deviation, S_x, given by,

$$S_x = \sqrt{\frac{1}{N-1}\sum_{i=1}^{N}(x_i - \bar{x})^2} \tag{5-2}$$

The mean value is the best estimate of the measured data. The uncertainty in the mean value due to random variations, with a confidence of 95%, can be estimated by the following.

$$P_{\bar{x}} = \frac{t_{95,\nu} S_x}{\sqrt{N}} \tag{5-3}$$

Where t_{95}, ν is the Student's t probability distribution function evaluated for a confidence interval of 95% and degrees of freedom, ν, given by,

$$\nu = N - 1 \tag{5-4}$$

The functional form of the t-distribution and associated tables for values of *t* are given by Lipson and Sheth (1973)

5.1.4 Calculate the Total Uncertainty of the Measured Value

In this step, the elemental and random uncertainties of the measured value are combined by the root-sum-square or RSS to determine the total uncertainty of the measured parameter. The RSS formula is given as,

$$u_x = \sqrt{(P_{\bar{x}})^2 + \sum_{i=1}^{n} \left(B_{x,i}\right)^2} \tag{5-5}$$

Where $B_{x,i}$ is the individual value of the elemental uncertainties.

5.1.5 Propagate the Uncertainty to the Final Result

The uncertainties of each measured value used to determine the uncertainty in a variable, *R*, that is a function of measured values, x_i. Kline and McClintock (1953) provide a valuable method for determining this uncertainty provided by,

$$u_R = \pm \sqrt{\sum_{i=1}^{L} \left(\left(\frac{\partial R}{\partial x_i}\Big|_{x=\bar{x}} \right) u_{x_i} \right)^2} \tag{5-6}$$

The above equation shows that the uncertainty of some calculated value *R* can be found by taking the partial derivative of *R* with respect to each of the parameters, x_i, of which *R* is a function. This partial derivative is evaluated for a value of x_i equal to the measured value of x_i . Each of these partial derivatives is then multiplied by the uncertainty of the measured value, u_{x_i}. The square root of the quadrature sum gives the final uncertainty for R.

5.2 Initial and Final Solution Mass Fractions

5.2.1 Elemental Uncertainty

The three directly measured values in this test were the solution mass, the solution volume and the solution temperature. Table 5-1: Elemental Uncertainties for Initial and Final Solution Mass Fractions shows the values and sources of the elemental uncertainty.

Table 5-1: Elemental Uncertainties for Initial and Final Solution Mass Fractions

	Mass [g]	**Volume [mL]**	**Temperature [°C]**
Elemental Uncertainty	0.5	0.3	0.2
Source of Uncertainty	Published uncertainty of scale	Published uncertainty of graduated cylinder	Published uncertainty of temperature probe

5.2.2 Total Uncertainty of the Measured Value

Since there is no random uncertainty associated with the measured values, the total uncertainty of the measured values is simply the elemental uncertainties shown in Table 5-1.

5.2.3 Propagate Total Uncertainties to the Final Calculated Value

The first value calculated from the primary measured values is the solution density. The partial derivative values of the solution density from Equation 5-6 are as follows:

$$\frac{\partial \rho}{\partial m} = \frac{1}{V} \tag{5-7}$$

and:

$$\frac{\partial \rho}{\partial V} = -\frac{m}{V^2} \tag{5-8}$$

Equations 5-7 and 5-8 are then evaluated at the mean value of the primary measurement, in this case at the mean value of mass and volume. Using Equation 5-6 the uncertainty of the density of the solution can be calculated. Table 5-2 lists the results of this process.

Table 5-2: Propagated Uncertainty Values for Solution Density

Value	Units	10% Before	10% After	30% Before	30% After	50% Before	50% After
$u_{\bar{\rho}}$	[g/L]	1.19	1.19	1.26	1.26	1.34	1.34

The uncertainty increases slightly as the nominal mass fraction increases due to the increase in measured mass per sample.

5.2.3.1 Mass Fraction

The solution density, in conjunction with the measured temperature values, can be used with the relation provided by Conde (Equation 4-1) to determine solution mass fraction. Equation 4-1 gives density as a function of mass fraction and temperature and so a regression similar to that depicted in Figure 4-3 is used to show mass fraction as a function of density and temperature. Table 5-3 shows the regression coefficients for mass fraction as a function of density and Table 5-4 shows the regression coefficients for mass fraction as a function of temperature. In each table, C0 is the constant coefficient, C1 is the coefficient for x and c2 is the coefficient for x^2.

Table 5-3: Regression coefficients for mass fraction as a function of density.

Nominal Solution	C0	C1	R^2
10% Before Boiling	-1.0827	0.0011	1
10% After Boiling	-1.0806	0.0011	1
30% Before Boiling	-0.9054	0.0009	1
30% After Boiling	-0.8934	0.001	1
50% Before Boiling	-0.8646	0.0009	1
50% After Boiling	-0.8229	0.0009	1

Table 5-4: Regression coefficients for mass fraction as a function of temperature

Nominal Solution	C0	C1	C2	R^2
10% Before Boiling	0.0989	8.23×10^{-5}	4.36×10^{-6}	1
10% After Boiling	0.0084	8.71×10^{-5}	4.33×10^{-6}	1
30% Before Boiling	0.3026	8.37×10^{-5}	4.52×10^{-6}	1
30% After Boiling	0.3007	8.34×10^{-5}	4.52×10^{-6}	1
50% Before Boiling	0.4215	8.46×10^{-5}	4.89×10^{-6}	1
50% After Boiling	0.4878	9.95×10^{-5}	4.88×10^{-6}	0.99

The equations of the regression curves can be used to determine the partial derivatives of the solution mass fraction with respect to solution density and solution temperature. These derivatives are evaluated at the mean value of the solution density and solution temperature and are used to calculate the uncertainty of the solution mass fraction which is shown in the table below.

Table 5-5: Uncertainties of Nominal Solution Mass Fractions

Value	Units	10% Before	10% After	30% Before	30% After	50% Before	50% After
$u_{\bar{\xi}}$	[-]	0.00131	0.00131	0.00114	0.00127	0.00121	0.00122

5.3 Pressure Analysis

As explained in Section 4.2 temperature measurements are used to determine the local mass fraction of solution at the location of each thermocouple. Here, the uncertainty of the mass fraction near each thermocouple as calculated in Section 4.2 is desired. As the partial derivatives and uncertainties are evaluated for each variable introduced in Section 4.2, Equation 5-6 is sequentially applied until the uncertainty of the mass fraction is determined. This process was repeated for all of the five thermocouples from which the solution mass fraction was determined. Table 5-6 lists the uncertainties of the mass fraction as a function of thermocouple and solution mass fraction.

Table 5-6: Average Mass Fraction Uncertainties for the Five Thermocouples and Three Nominal Mass Fractions Over the Boiling Time Period

Nom. ξ	$u_{\xi 1}$	$u_{\xi 2}$	$u_{\xi 3}$	$u_{\xi 4}$	$u_{\xi 5}$
10%	0.0072	0.0074	0.0074	0.0077	0.0074
30%	0.001858	0.001929	0.00198	0.001976	0.001926
50%	0.001005	0.001011	0.001013	0.001021	0.001025

5.4 Solar Incidence

Starting with the uncertainty of the two basic solar angles from the SRRL and the uncertainty of the slope and azimuth of the tube, the process outlined by Equation 5-6 can also be used to determine the uncertainty of the incidence angle on the evacuated tube. Using this process, the uncertainties in the incidence angle of the sun on the evacuated tube are found to be between 2.5 and 3.5 degrees.

5.5 Evaporated Water

The crux of the entire analysis of solar and temperature data is to arrive at an amount of water evaporated during the period of time in which the solution was boiling. As explained in Section 4.3.6.4, the efficiency curve for the collector defined by Equation 4-29 is used to calculate the amount of water

boiled. This equation effectively takes all of the measured temperature and solar data and reduces it to a linear equation. As such it also reduces all of the uncertainties for the measured values and it is both reasonable and prudent to perform an uncertainty analysis on the parameters m and η_{max} that define the tubular efficiency as a function of temperature difference over incident solar radiation.

First to be discussed is the linear regression method used to determine m and η_{max}. In a general linear equation given by,

$$\hat{y} = f(x) = Mx + \eta_{max} \tag{5-9}$$

$\hat{y}$ is the calculated η, , x is the temperature difference between the solution and ambient divided by incident radiation. Using a series of data which is calculated from the measured values in Section 4, a and b can be calculated with the following two equations:

$$a = \left[n\sum_{i=1}^{N} x_i y_i - \left(\sum_{i=1}^{N} x_i\right)\left(\sum_{i=1}^{N} y_i\right)\right] / \left[n\sum_{i=1}^{N} x_i^2 - \left(\sum_{i=1}^{N} x_i\right)^2\right] \tag{5-10}$$

$$b = \left[\left(\sum_{i=1}^{N} y_i\right)\left(\sum_{i=1}^{N} x_i^2\right) - \left(\sum_{i=1}^{N} x_i\right)\left(\sum_{i=1}^{N} x_i y_i\right)\right] / \left[\left(n\sum_{i=1}^{N} x_i^2\right) - \left(\sum_{i=1}^{N} x_i\right)^2\right] \tag{5-11}$$

What is desired however is an uncertainty for $\hat{y}$ which can be used to calculate an uncertainty of water boiled for each time step, which in turn, can be used to give an overall uncertainty of the water boiled during a particular test. The uncertainty of $\hat{y}$ or $\boldsymbol{u}_{\hat{y}}$ is given by,

$$\boldsymbol{u}_{\hat{y}} = \pm t_{\alpha,N-2}\sigma_{x,y}\sqrt{\frac{1}{N} + \frac{(x_0 - x_m)^2}{S_{xx}}} \tag{5-12}$$

Where $t_{\alpha,n-2}$ is the t distribution factor of α desired confidence and $N-2$ degrees of freedom, x_0 is the predictor variable, $\sigma_{x,y}$ given by,

$$\sigma_{x,y} = \sqrt{\sum_{i=1}^{N} \frac{(y_i - \hat{y}_i)^2}{N-2}} \tag{5-13}$$

x_m given by,

$$\sigma_{x,y} = \sum_{i=1}^{N} \frac{x_i}{N} \tag{5-14}$$

and S_{xx} given by,

$$\sigma_{x,y} = N\left(\sum_{i=1}^{N} x_i^2\right) - \left(\sum_{i=1}^{N} x_i\right)^2 \tag{5-15}$$

The term y_i is the efficiency for each time step calculated from measured data and $\hat{y}_i$ is the efficiency for each time step as predicted by the linear regression.

Using the method outlined, the regression parameters as well as the uncertainty of the predicted value can be calculated for the three nominal mass fractions. These parameters are displayed below in Table 5-7. The value of the uncertainty of the water boiled for the 50% solution batch is lower than the other two nominal solutions because less water was evaporated in that test than the other two.

Table 5-7: Regression Coefficients and Uncertainty of Water Boiled per Batch of Nominal Mass Fraction Solution

	a	**b**	$\boldsymbol{u_{H_2O,Boiled}}$ **[g]**
10%	-3.575	0.898	0.856
30%	-3.304	0.918	0.886
50%	-3.445	0.955	0.551

Since all three batches of solution were regenerated in a single tube, and the performance of the single tube is desired, all of the data points for all three of the mass fraction batches were regressed as a group. In addition, the uncertainty of the efficiency for the entire data set was calculated. These values

were used to determine the amount of water boiled for each nominal mass fraction the results of which will be discussed in the following chapter. For now, Table 5-8 displays the regression coefficients and uncertainty of water boiled per batch of nominal mass fraction using the regression of all data points

Table 5-8: Regression Coefficients and Uncertainty of Water Boiled per Batch of Nominal Mass Fraction Solution Using Overall Regression

a	b	10% $u_{H_2O,Boiled}$ [g]	30% $u_{H_2O,Boiled}$ [g]	50% $u_{H_2O,Boiled}$ [g]
-2.743	0.893	1.16	1.02	0.79

5.6 Uncertainty of Solution Left in Apparatus

It should be noted before results are discussed that there is another source of error that occurs with this data collection for which quantification is difficult. This uncertainty is the amount of solution that remains inside the evacuated tube after the solution is poured out. What makes this uncertainty difficult to quantify is the fact that it is heavily reliant on the surface tension and viscosity of the solution being regenerated. For low mass fraction solutions, the surface tension and viscosity are low. As a result, when the solution is poured from the evacuated tube it is less apt to stick to the walls of the tube and the thermocouples. When the solution is more concentrated, it has higher viscosity and surface tension and is more likely to stick to apparatus components. This was empirically observed when the thermocouples were removed from the evacuated tube to pour out the 50% solution. In addition to sticking to the walls of the evacuated tube and thermocouples, the solution can stick to the walls of the jug used to haul the solution to and from the apparatus as well as the beaker used to pour the solution into the volumetric flask.

Taking this into consideration, a side-experiment was conducted to quantify the amount of solution that was being lost to the above mentioned processes. This experiment was to weigh a sample of a particular sample, pour the sample into the apparatus, pour the sample out of the apparatus and weigh it.

The difference in weight is the amount of solution that is naturally left in the apparatus. For each test, the apparatus was allowed to fully dry. The results are as follows:

Table 5-9: Solution mass left in apparatus

10% Solution	**30% Solution**	**50% Solution**
13.5g	17.5g	26g

The amount of solution left in the apparatus for the 50% nominal solution is greater than the other two because there is a significant change in the solution properties from 30% to 50%. This uncertainty is also a bias error meaning that it will only act to increase the measured difference in solution mass from initial to final states. The implications of this error will be further discussed in the next chapter.

6 RESULTS AND DISCUSSION

From the previous sections, raw data from experimental measurement was analyzed to determine if liquid desiccants could be regenerated in evacuated tubes. The following sections provide detail to the results of that analysis as well as a discussion to the significance of the results. The figure below is an example of the temperature inside the tube as a function of time which was the basis for this analysis

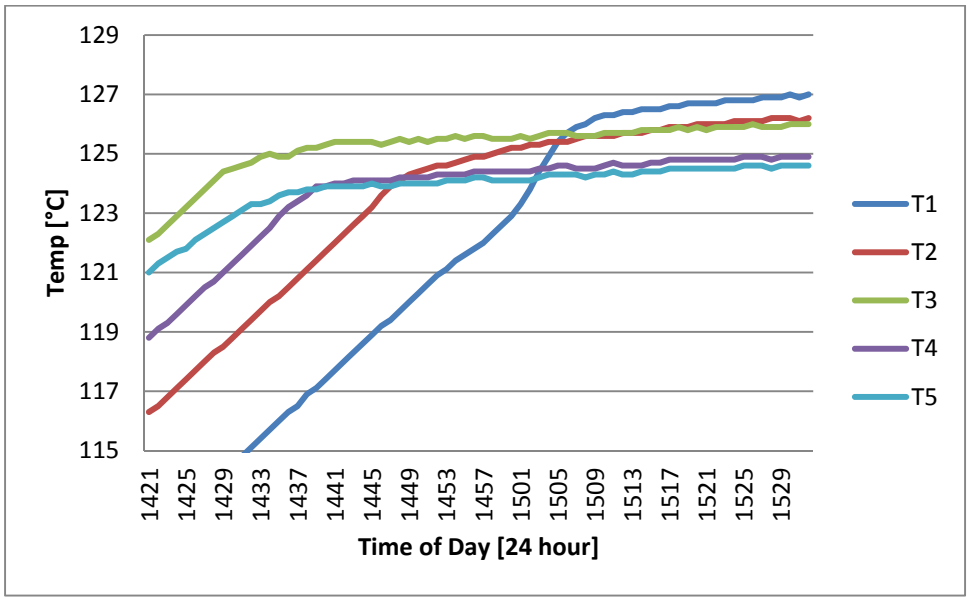

Figure 6-1: Temperature as a Function of Time for the Five Thermocouples Inserted in the Evacuated Tube for a 50% Nominal Solution

6.1 Mass Fraction from Direct Measurement

Table 6-1 to Table 6-3 show the initial mass fractions calculated from mass, volume and temperature using the relation by Conde for a 10%, 30% and 50% nominal solution.

Table 6-1: Initial Solution Properties for 10% Nominal Solution

Mass [g]	Volume [mL]	Temp [°C]	ρ_{sol} [kg/m^3]	τ	ρ_{H2O} [kg/m^3]	ξ
543.5	500	24.0	1087.0	0.54	997.3	0.1025
543.5	500	24.0	1087.0	0.54	997.3	0.1025
544.5	500	24.0	1089.0	0.54	997.3	0.1047
543.5	500	24.0	1087.0	0.54	997.3	0.1025
543.5	500	24.0	1087.0	0.54	997.3	0.1025

Table 6-2: Initial Solution Properties for 30% Nominal Solution

Mass [g]	Volume [mL]	Temp [°C]	ρ_{sol} [kg/m^3]	τ	ρ_{H2O} [kg/m^3]	ξ
644.0	500	35.6	1288.0	0.52	993.8	0.3089
644.5	500	34.8	1289.0	0.52	994.1	0.3095
645.5	500	34.0	1291.0	0.53	994.4	0.3111
645.5	500	33.8	1291.0	0.53	994.5	0.3110
646.0	500	33.7	1292.0	0.53	994.5	0.3119

Table 6-3: Initial Solution Properties for 50% Nominal Solution

Mass [g]	Volume [mL]	Temp [°C]	ρ_{sol} [kg/m^3]	τ	ρ_{H2O} [kg/m^3]	ξ
739.0	500	45.7	1478.0	0.51	989.9	0.4890
737.5	500	45.2	1475.0	0.51	990.1	0.4860
739.0	500	44.2	1478.0	0.51	990.6	0.4881
739.5	500	43.2	1479.0	0.51	991.0	0.4885
593.5	400	43.0	1483.8	0.51	991.1	0.4927

Table 6-4, Table 6-5 and Table 6-6 show the sample data for the final solutions of the nominal mass fraction batches. Since these samples were measured directly after boiling, the temperatures can be noticed to be significantly higher than for the initial samples. It should be also noticed that the mass and volume of the fifth samples for each sample set are less than the fifth sample in the initial solution data.

This shows that there WAS boiling and that water was evaporated from the tube. The final mass fractions for each nominal value can be seen to increase from the initial to the final state.

Table 6-4: Final Solution Properties for 10% Nominal Solution

Mass [g]	**Volume [mL]**	**Temp [°C]**	**ρ_{sol} [kg/m^3]**	**τ**	**ρ_{H2O} [kg/m^3]**	**ξ**
536.5	500	61.2	1073.0	0.4833	982.6	0.1047
537.0	500	61.8	1074.0	0.4824	982.3	0.1062
537.5	500	60.0	1075.0	0.4852	983.2	0.1062
537.0	500	58.6	1074.0	0.4873	983.9	0.1042
275.5	255	55.3	1080.4	0.4924	985.6	0.1093

Table 6-5: Final Solution Properties for 30% Nominal Solution

Mass [g]	**Volume [mL]**	**Temp [°C]**	**ρ_{sol} [kg/m^3]**	**τ**	**ρ_{H2O} [kg/m^3]**	**ξ**
643.5	500	82.9	1287.0	0.4498	970.0	0.3377
643.5	500	78.8	1287.0	0.4561	972.6	0.3344
643.5	500	78.2	1287.0	0.4570	972.9	0.3339
646.0	500	72.9	1292.0	0.4652	976.1	0.3347
388.5	300	71.6	1295.0	0.4672	976.9	0.3366

Table 6-6: Final Solution Properties for 50% Nominal Solution

Mass [g]	**Volume [mL]**	**Temp [°C]**	**ρ_{sol} [kg/m^3]**	**τ**	**ρ_{H2O} [kg/m^3]**	**ξ**
744	500	72.8	1488.0	0.4654	976.2	0.5168
755	500	68.5	1510.0	0.4720	978.6	0.5331
738.5	500	67.1	1477.0	0.4742	979.4	0.5024
748.5	500	66.6	1497.0	0.4750	979.7	0.5201
427	287	62.4	1487.8	0.4815	982.0	0.5087

The data displayed in Table 6-1 through Table 6-6 shows the initial and final solution data taken for the three nominal mass fraction solutions. Table 6-7 below is a summary of those tables that shows the total mass rather than the mass of each individual sample.

Table 6-7: Summary of Directly Measured Mass Fraction Data

	Initial Mass [g]	Final Mass [g]	Δmass [g]	ξ,start	ξ,finish	Δξ
10%	2652	2443	209	0.1029	0.1061	0.0032
30%	3149	2979	170	0.3105	0.3355	0.0250
50%	3549	3413	136	0.4888	0.5162	0.0274

It can be seen from the final column of Table 6-7 that the mass fraction for each batch of solution increased from start to finish. Figure 6-2, Figure 6-3 and Figure 6-4 give a graphical representation of the initial and final solution mass fractions. Also included in the figures are the 95% confidence interval error bars.

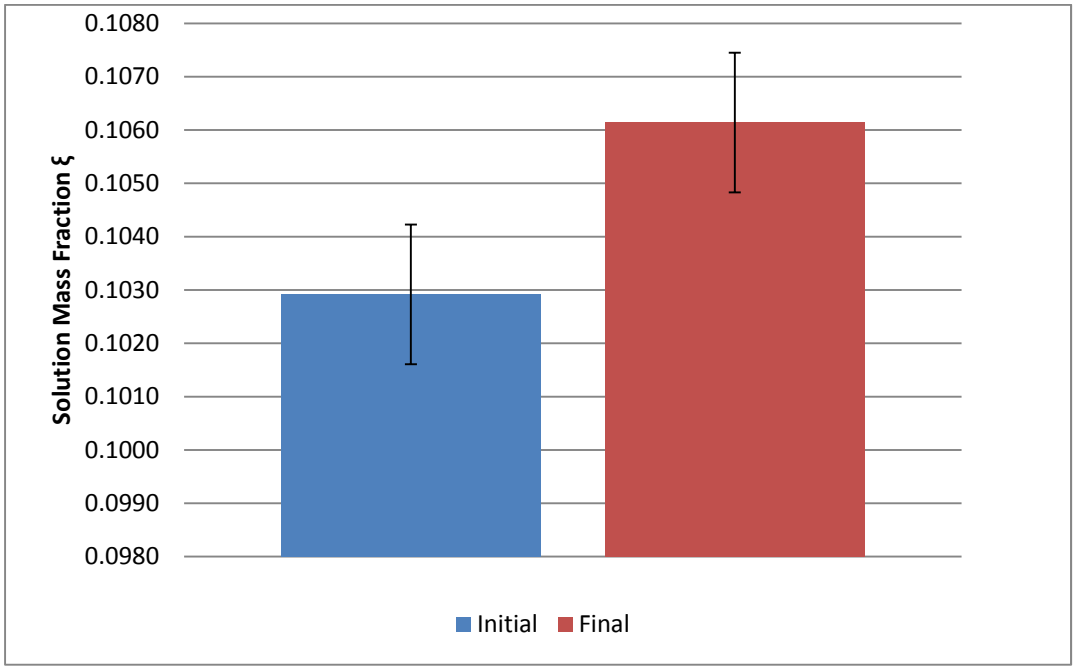

Figure 6-2: Initial and Final Mass Fractions for 10% Nominal Mass Fraction Solution

Figure 6-2 shows the initial and final mass fractions for a 10% nominal mass fraction solution. For the 10% nominal mass fraction batch, the solution started at 0.1029 and ended at 0.1069. This shows an increase in mass fraction of 0.0032. Compared to the 95% confidence interval for the final solution of ± 0.00131, this increase is shown to be significant. The lack of a large change in mass fraction however,

can be attributed to the low initial mass fraction. At low mass fractions, a larger amount of water is required to be evaporated to achieve similar mass fraction changes than at higher mass fractions.

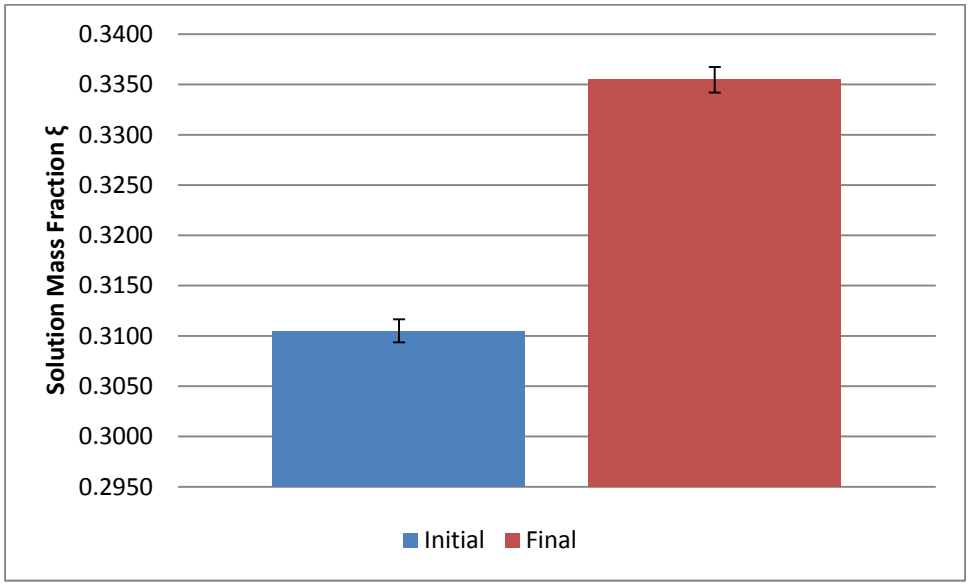

Figure 6-3: Initial and Final Mass Fractions for 30% Nominal Mass Fraction Solution

Figure 6-3 shows the initial and final mass fractions of a 30% nominal mass fraction batch. For this batch the solution starts at a mass fraction of 0.3105 and ends at a mass fraction of 0.3355 giving a change in mass fraction 0.0250. When compared to the 95% confidence interval of the initial and final solutions of ± 0.00114 and ± 0.00127 respectively, this is a significant increase in mass fraction.

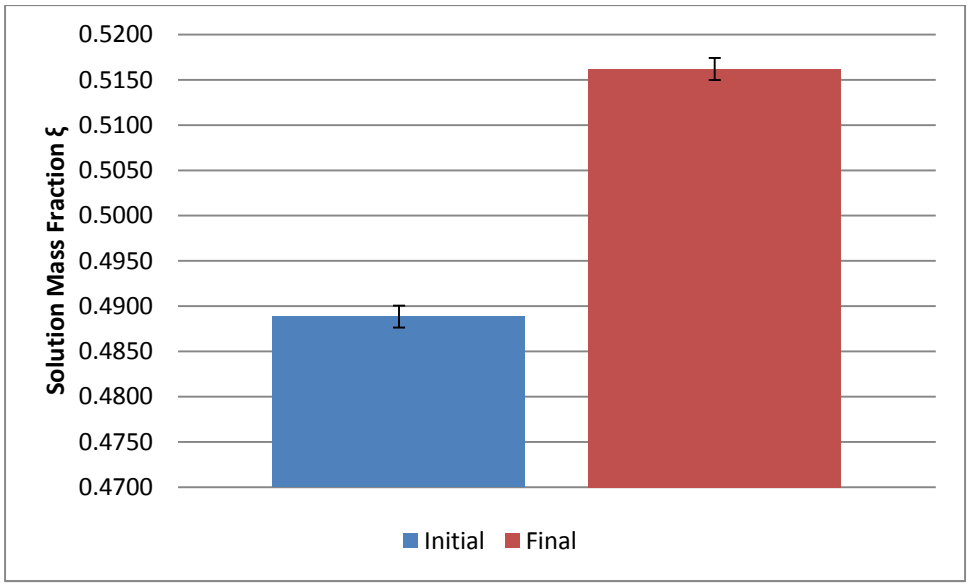

Figure 6-4: Initial and Final Mass Fractions for 50% Nominal Mass Fraction Solution

Figure 6-4 shows the initial and final solution mass fractions of a 50% nominal mass fraction batch. For this batch, the solution starts at a mass fraction of 0.4888 and finishes with a mass fraction of 0.5162 for a change in mass fraction of 0.0274. When compared to the 95% confidence interval of the final solution of $\pm$ 0.00122 this change in solution mass fraction is statistically significant. The 95% confidence interval of the initial solution is $\pm$0.00121.

From Figure 6-2 to Figure 6-4 it can be seen that there was significant desiccant regeneration for all nominal mass fraction solutions. This result is however achieved from the solution after it has been poured out of the tube and thoroughly mixed. Also of concern is whether or not the solution stratifies by mass fraction inside the tube. The more dense, higher mass fraction solution remaining in the bottom while the lighter, lower mass fraction, and easier to regenerate portion stays near the top. The following section discusses what indeed happens as the solution regenerates

6.2 Pressure Analysis

In the preceding section, it was shown that liquid desiccant was regenerated in an evacuated tube. Since the analysis only focused on the bulk solution properties of the initial and final states, and there was concern that desiccant could be crystallizing on the bottom of the evacuated tube, further analysis is needed to determine if the solution was indeed regenerating or concentrated solution was just sinking to the bottom of the tube.

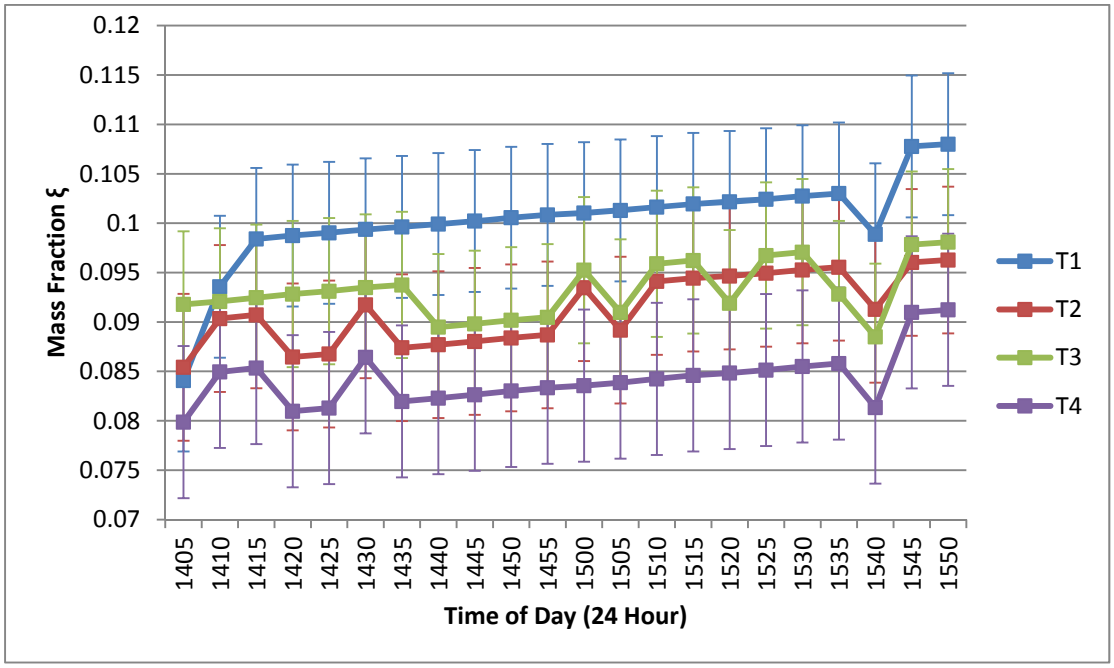

Figure 6-5: Mass Fraction as a Function of Time for a 10% Nominal Mass Fraction Solution during Boiling

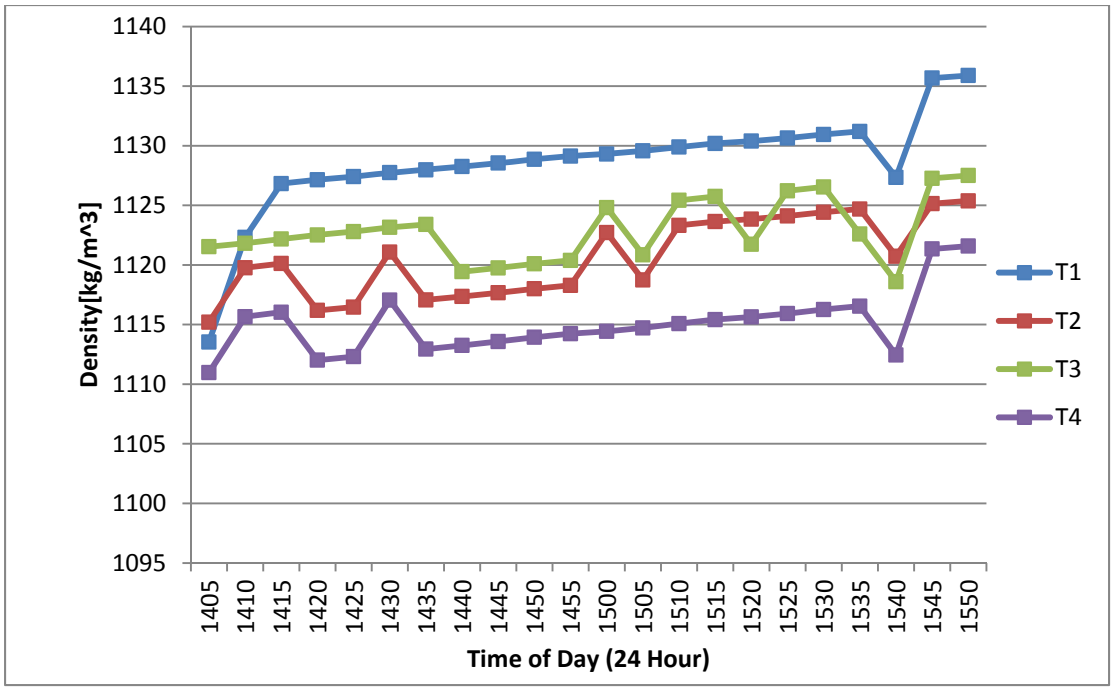

Figure 6-6: Density as a Function of Time for a 10% Nominal Mass Fraction Solution during Boiling

Figure 6-5 shows the mass fraction and Figure 6-6 shows the density of the 10% solution as it regenerates during boiling. These charts were created through the analysis in Chapter 4.2. Thermocouple 1, depicted in the chart legend as T1 is the bottom most thermocouple. T4 is the second thermocouple from the top of the tube. Only thermocouples 1 through 4 are charted as thermocouple 5 becomes unwhetted during regeneration. It can be seen that the mass fraction and density at each one of the thermocouples is increasing during regeneration. There does appear to be a slight amount of mass fraction stratification between the bottom of the tube and the top as T1 has approximately 0.015 greater mass fraction than T4. This stratification difference is larger than the displayed increase in mass fraction over the time period of approximately 0.012. The 95% confidence interval for this nominal mass fraction solution is much larger than the other batches. This is because the partial derivative of mass fraction with respect to temperature is much more sensitive to uncertainties in temperature than the other mass fractions due to the slope of the line of the empirical curve derived by Conde.

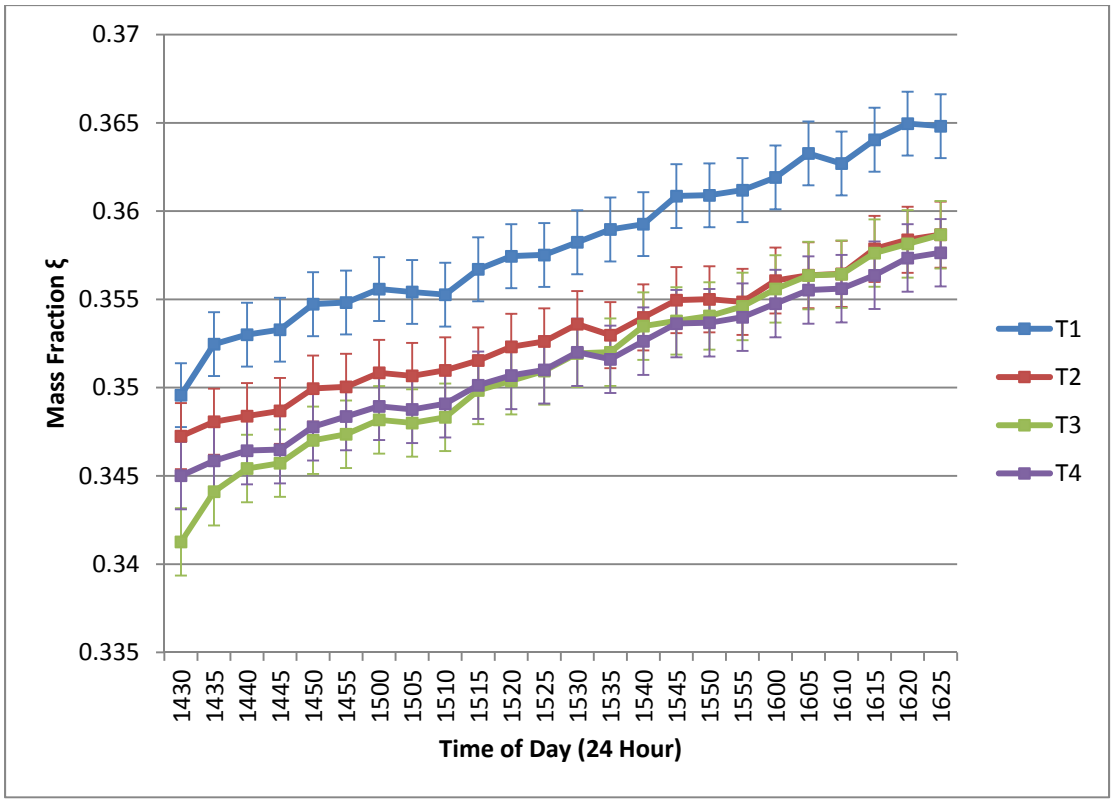

Figure 6-7: Mass Fraction as a Function of Time for a 30% Nominal Mass Fraction Solution during Boiling

Figure 6-7 shows the change in mass fraction for each thermocouple as a function of time during regeneration for the 30% nominal mass fraction solution. Compared to the uncertainty bars in Figure 6-5, the error bars shown above are much smaller. The average error is 0.002 as opposed to 0.007. It can be seen that the solution regenerates and a much higher rate than the error. For this solution there is also less stratification for thermocouples 2 3 and 4 than there was for a 10% nominal solution. It can be seen that thermocouple 1 has a bit higher mass fraction than the other thermocouples but the increase in mass fraction is of the same magnitude as the others.

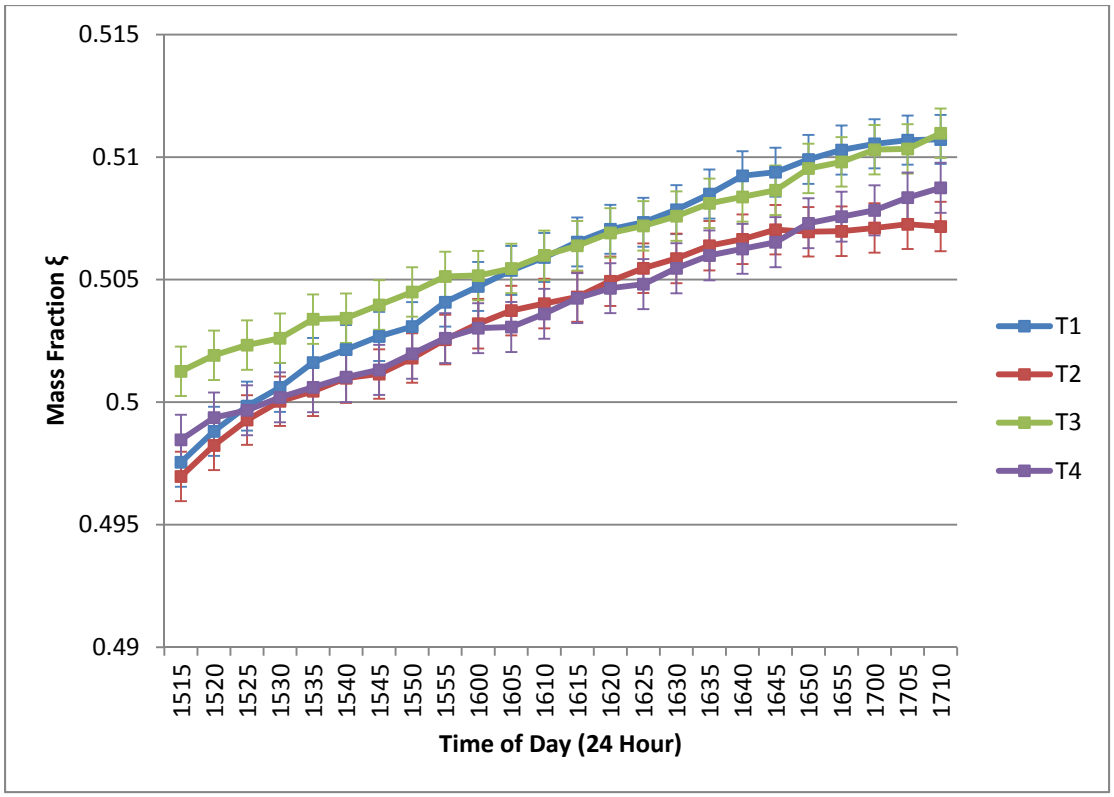

Figure 6-8: Mass Fraction as a Function of Time for a 50% Nominal Mass Fraction Solution during Boiling

Figure 6-8 shows the increase in mass fraction for the 50% nominal mass fraction solution. The average mass fraction error as displayed by the error bars is approximately 0.001. The 50% nominal solution is the least stratified out of the three batches tested. It can be seen in Figure 6-8 that the average difference in mass fraction between thermocouples for any time step is 0.005 which is about half of the change in mass fraction from start to finish of the boiling period of about 0.01. For the 50% solution it should also be noted that thermocouple 1 is not, over the period, more concentrated than the other thermocouples. This is interesting as it was originally theorized that stratification would be worse for the higher mass fraction solutions as these are closer to the crystallization point of the solution.

Overall, Figure 6-5, Figure 6-7 and Figure 6-8 show that stratification of the solution inside the tube does not increase as regeneration occurs. It can also be seen that stratification actually decreased

with an increase in nominal solution mass fraction. It is interesting to notice that the initial and final mass fractions of the solution predicted by the pressure analysis match up fairly well with the measured mass fractions of the solutions as displayed in Table 6-7. This is notable because the mass fractions predicted by the pressure analysis were determined from completely independent data from the directly measured mass fraction. This fact validates the method used for the pressure analysis.

6.3 Incident Radiation

The incidence angle of direct radiation on an evacuated tube is a critical parameter in determining how much an evacuated tube can regenerate liquid desiccants. A brief discussion of the incidence angle on an evacuated tube as compared to an incidence angle on a flat plate collector is justified.

Figure 6-9 shows the incidence angle on a tubular collector versus the incidence angle on a flat plate collector at the same tilt as the axis of the tube. The day for which incidence angles are displayed is September 27th 2009 which is five days after the autumnal equinox. It can be seen in Figure 6-9 that the incidence angle of a planar collector decreases until it reaches a minimum at solar noon. The incidence angle of a tubular collector actually increases until solar noon and then decreases after. This is due to the zenith angle of the sun, which, near the equinox is approximately the latitude at the location or 40 degrees, is greater than the tilt of the tube. Over the course of a day however, the incidence angle for a tube is much less than the incidence for a flat plate. Since evacuated tubes, like most solar collectors, get the majority of their energy from direct radiation, this can make a large difference in the long term performance of evacuated tubes as devices for regenerating liquid desiccants.

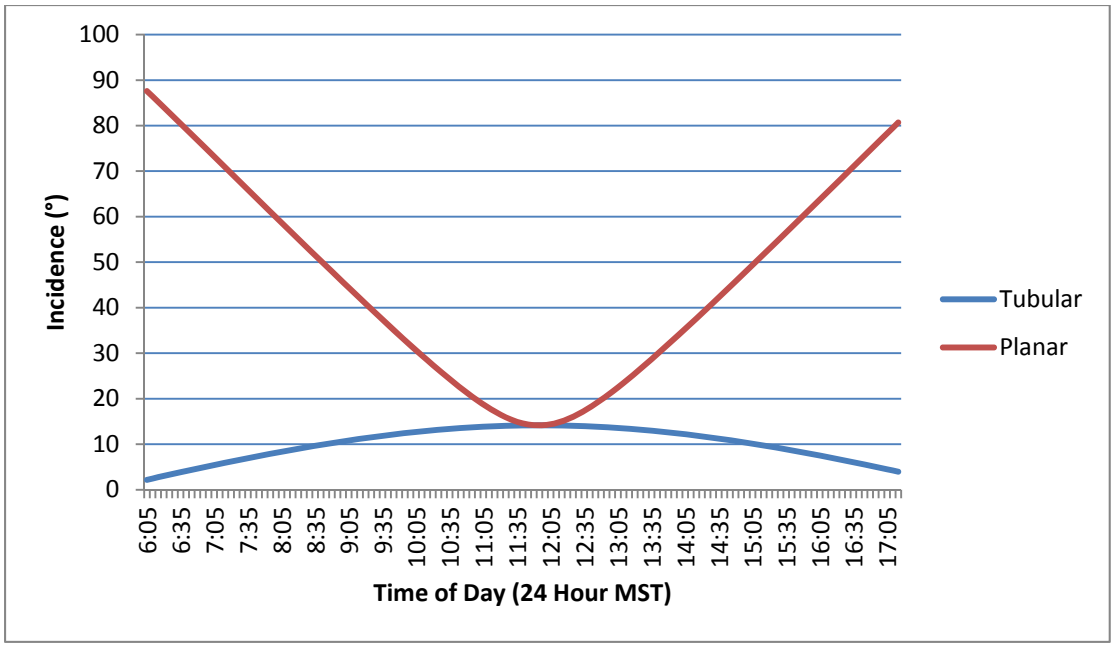

Figure 6-9: Incidence Angle on Tube and Plane Parallel to Axis of Tube as a Function of Time for September 27th 2009

Figure 6-10, Figure 6-11 and Figure 6-12 show the components of radiation incident on an evacuated tube for the 10% nominal test, 30% nominal test, and the 50% nominal test respectively. It can be seen that the vast majority of total radiation incident in all cases is direct. This equates to approximately 950 W/m^2 at solar noon. A little more than 200 W/m^2 can be attributed to other sources. Except for the 10% case, which had a slight dip in direct radiation at 11:00 AM MST, the radiation for all cases came from perfectly clear skies throughout testing. Constant radiation was required to achieve reasonable efficiency results because effectively accounting for variable radiation, such as the radiation available during partly cloudy testing proved impossible.

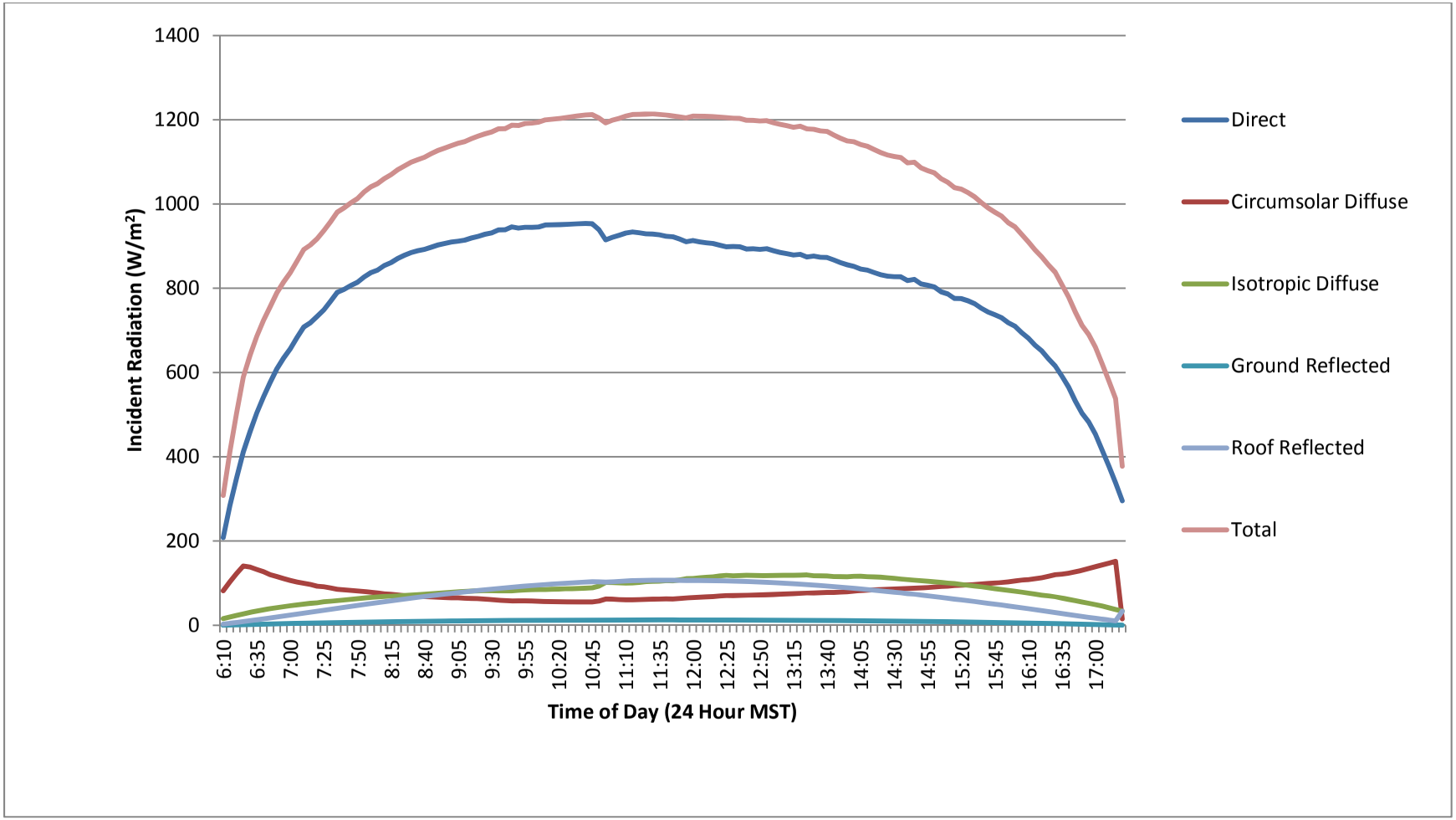

Figure 6-10: Components of Radiation Incident on Tube During 10% Nominal Mass Fraction Test

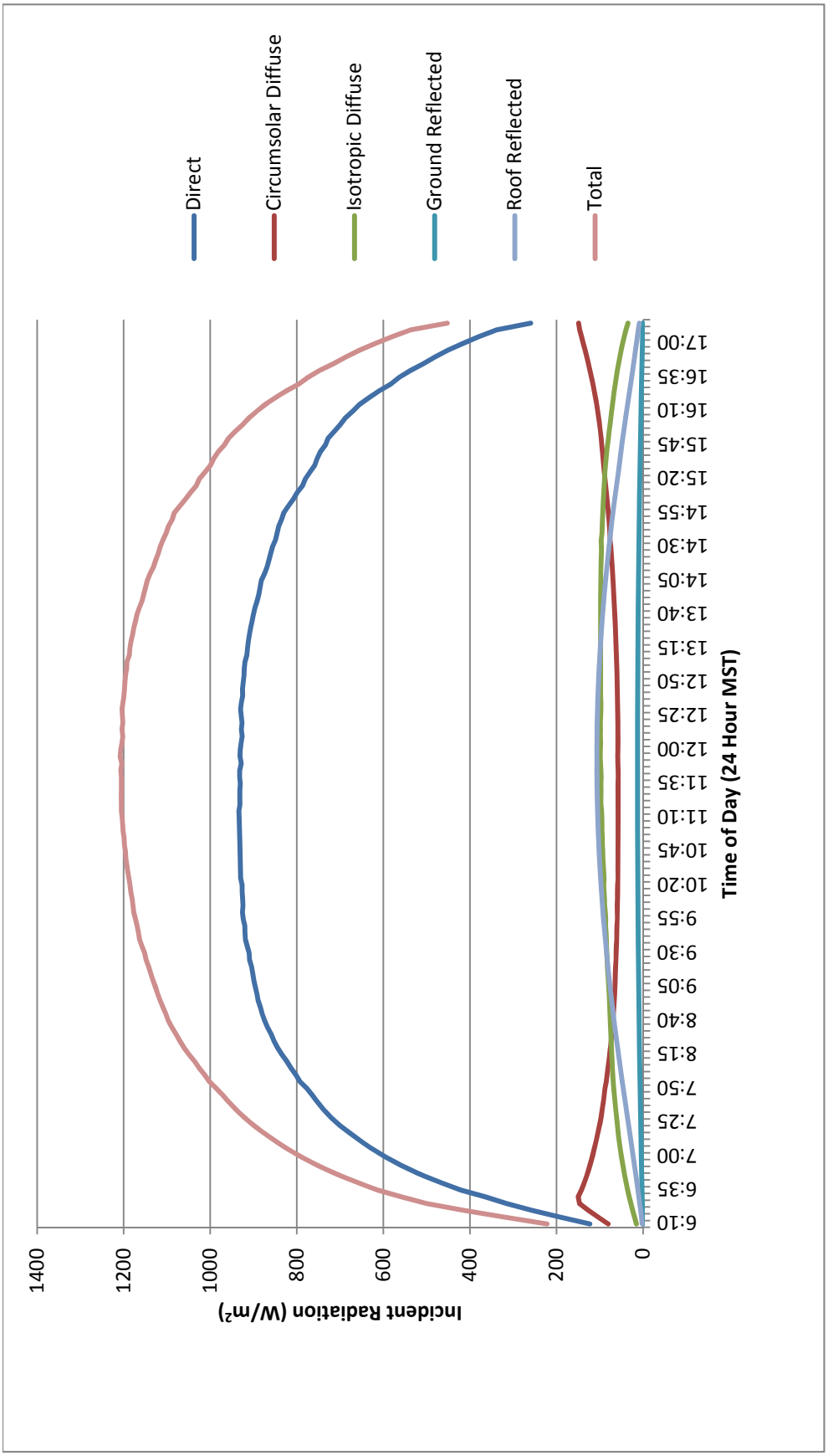

Figure 6-11: Components of Radiation Incident on Tube During 30% Nominal Mass Fraction Test

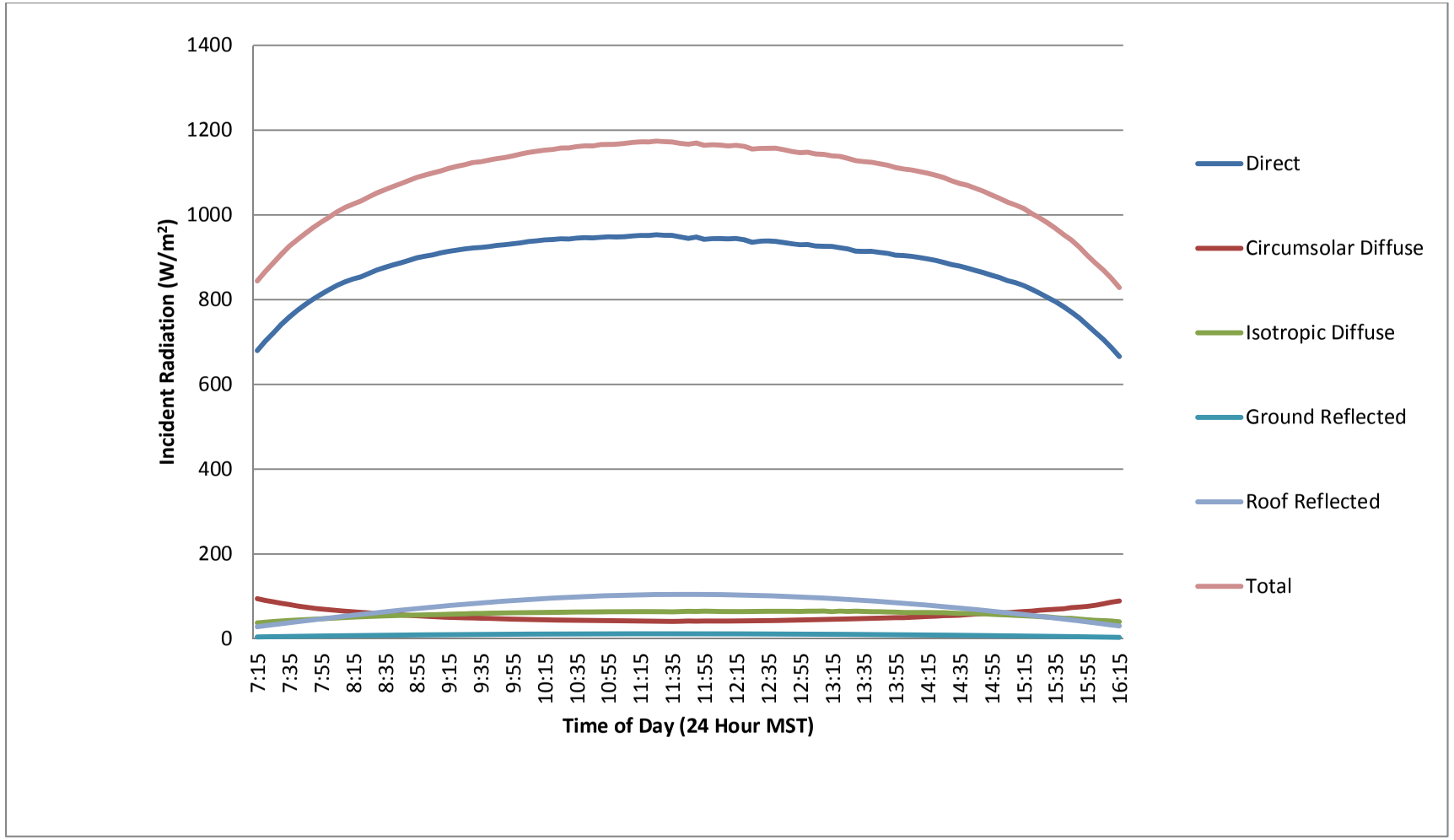

Figure 6-12: Components of Radiation Incident on Tube During 50% Nominal Mass Fraction Test

6.4 Efficiency Curves

Using the method outlined in Section 4.3.6.4, the efficiency curves for the various tests are created. Figure 6-13, Figure 6-14 and Figure 6-15 show the efficiency curves for the 10%, 30% and 50% nominal mass fraction solutions respectively. Figure 6-16 shows all three data sets on the same plot. The x-axis of the plots is the temperature difference of the solution and the ambient air over the incident radiation on the tube while the y-axis shows the tube efficiency. The internal tube temperature is the average of the five thermocouples in the tube weighted by the volume of solution that they are intended to measure. Included with the data plots are the linear regression lines and equations for each set of data. Also shown on the charts is the 95% confidence interval, with the green line showing the upper limit, and the red line showing the lower limit of confidence. The equations of the linear regression show that the slopes of the lines are fairly similar. There does appear to be a statistically significant difference in the y-intercept of the lines, or the maximum efficiency of the tubes. This difference could potentially be attributed to secondary effects arising from the natural convection inside the tube that is dependent on viscosity and density of the solution. It can be seen when looking at Figure 6-16 the 95% confidence interval calculated using the aggregate of data is larger than the 95% confidence interval of the individual data sets. This again can be attributed to the differences described above. Figure 6-17 is a similar plot to Figure 6-16 except that the regression equation displayed is the regression for the aggregate data. This is the regression used to calculate the water boiled using the aggregate model which is discussed below. Also included in this chart are the published efficiency curves for two commercially available collectors that use the same evacuated tube design, but differ in the way that the working fluid is heated. The curve shown by the dashed orange line represents a collector where the working fluid is passed through the evacuated tube by a U-shaped copper tube that runs down and back the length of the evacuated glass tube. In the dashed purple line, the working fluid doesn't pass into the tube at all. Instead, a heat pipe is installed inside the evacuated tube and the working fluid is heated by the bulb of the heat pipe which is

inserted into a pressurized header. In this type of collector, the working fluid can be water at mains pressure. The lower efficiencies of the heat pipe style collector represent the efficiencies lost through the heat pipe and the heat transfer from the bulb to the working fluid. The U-shaped collector curve shows higher efficiencies than the tested apparatus due to the fact that the fluid temperature on the x-axis is an entering fluid temperature rather than an average overall temperature.

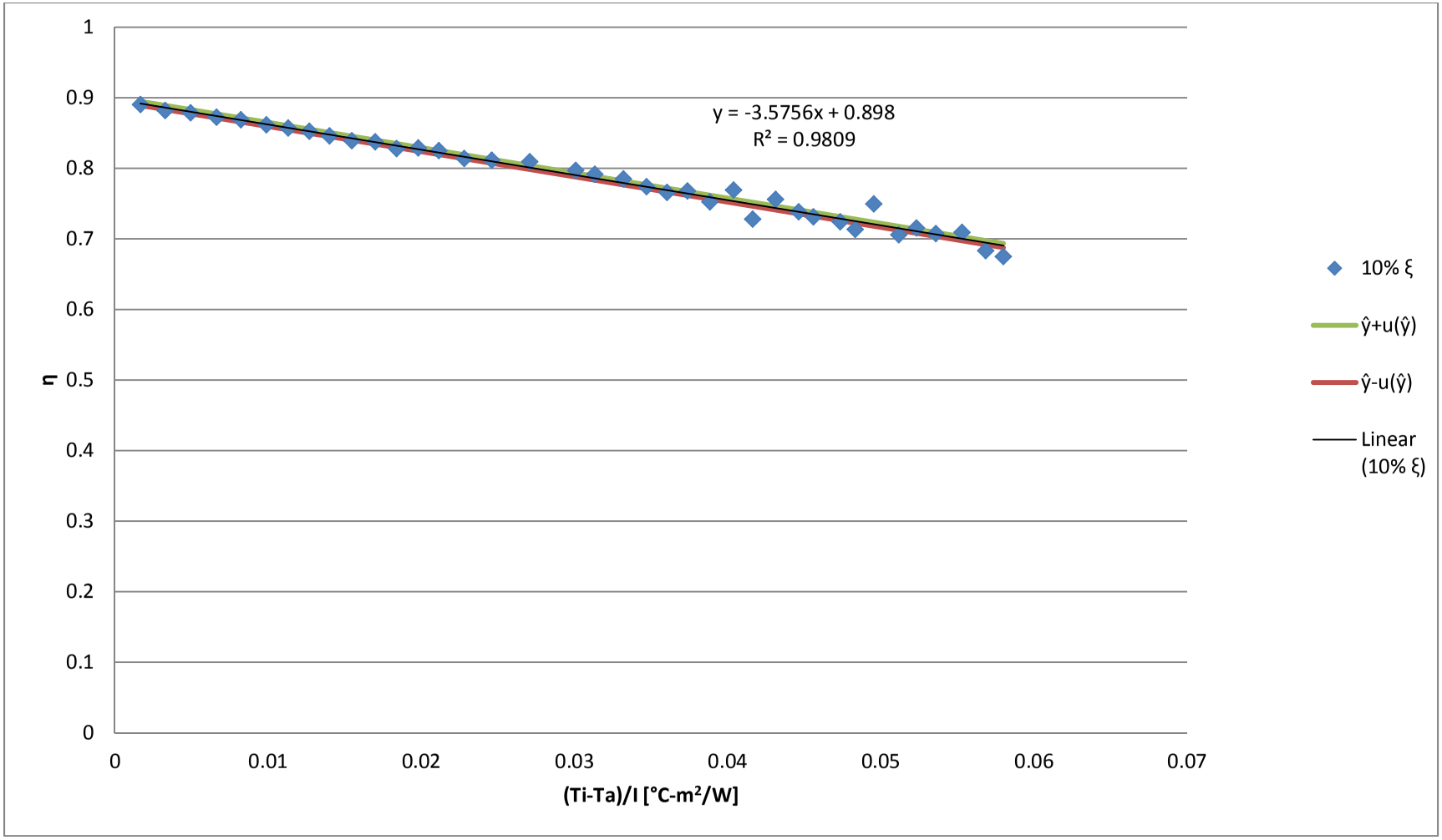

Figure 6-13: Efficiency Plot with Regression Line for 10% Nominal solution

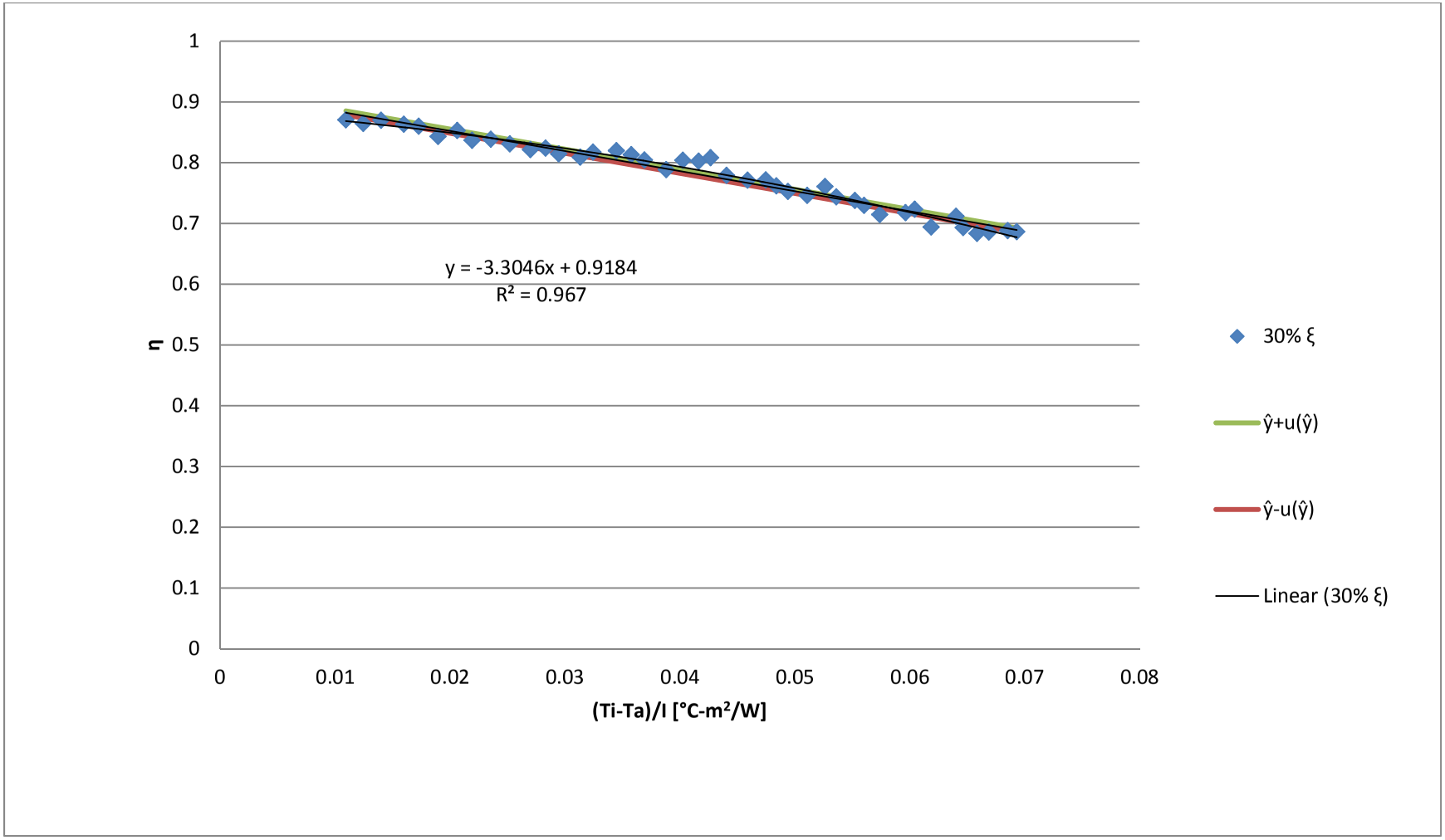

Figure 6-14: Efficiency Plot with Regression Line for 30% Nominal solution

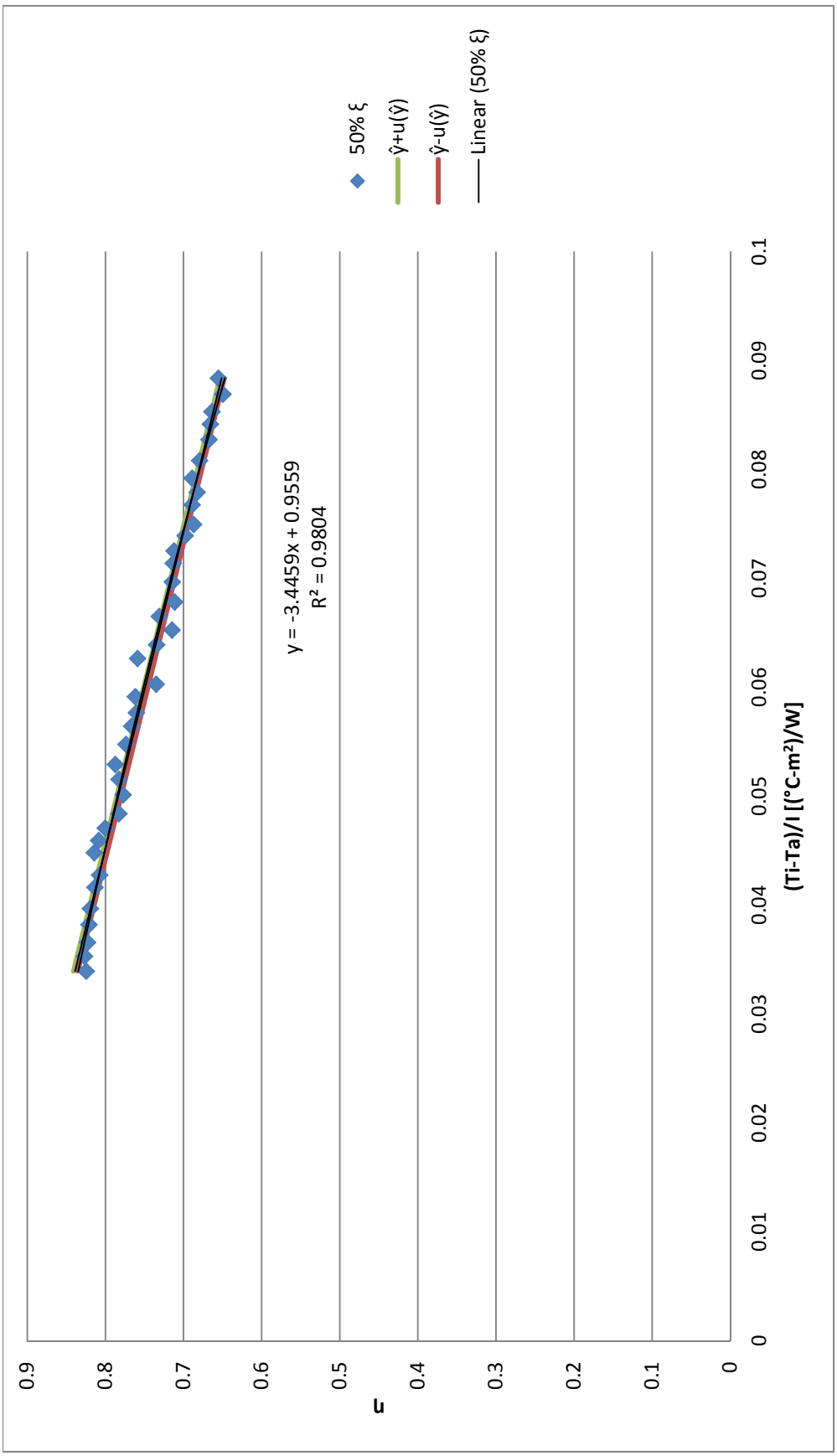

Figure 6-15: Efficiency Plot with Regression Line for 50% Nominal solution

Figure 6-16: Efficiency Plot of All Solution Mass Fractions Plotted Separately with 95% Confidence Intervals

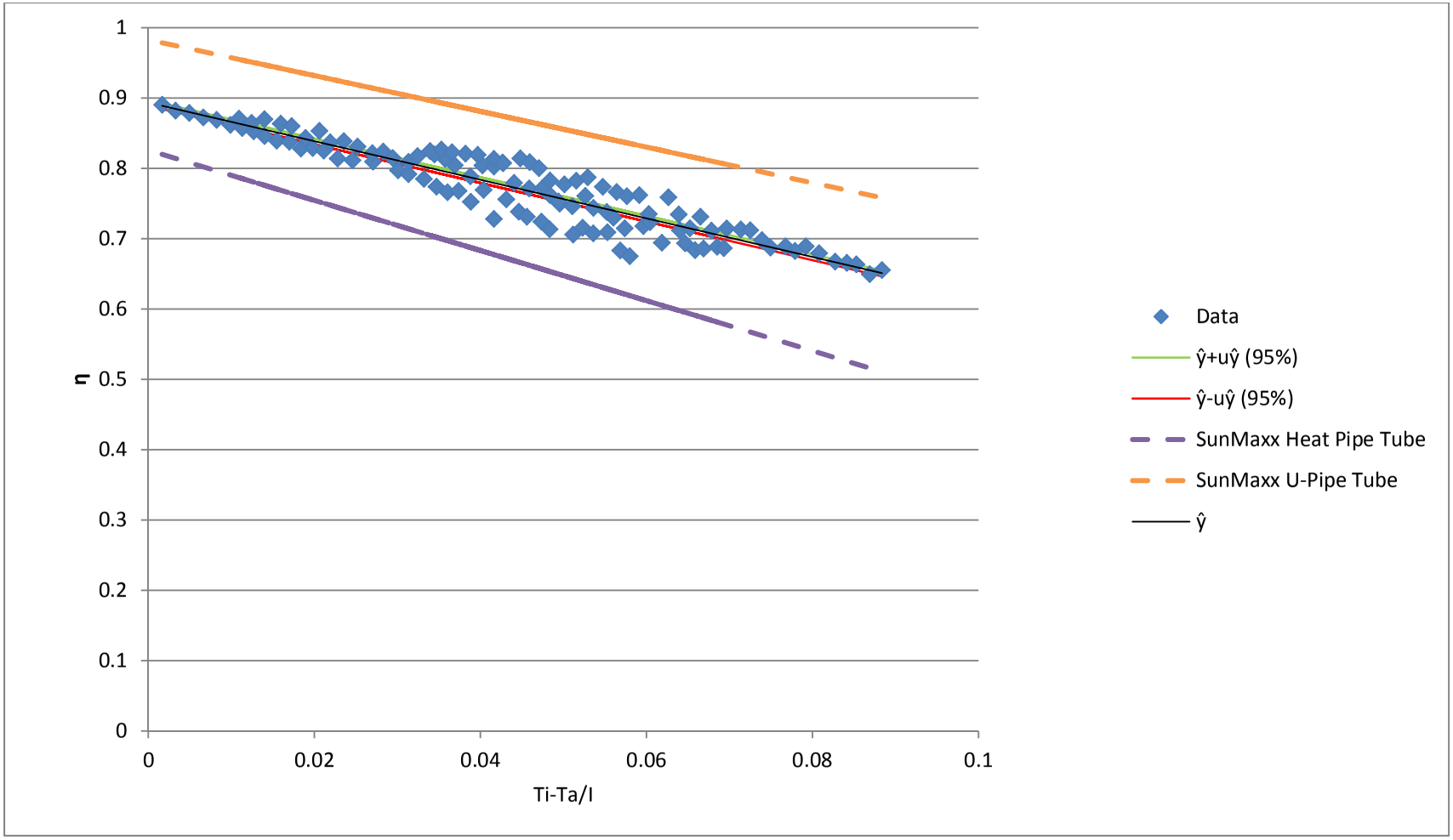

Figure 6-17: Efficiency Plot of All Solution Mass Fractions with 95% Confidence Intervals

6.5 Evaporated Water

Using the efficiency curves described above, the amount of water evaporated during regenerated is calculated using the method described in Section 4.3.7. This amount, as predicted by the tube model is then compared to the amount of water evaporated as determined by direct measurement. Figure 6-18 below shows this comparison for the 10% nominal mass fraction solution.

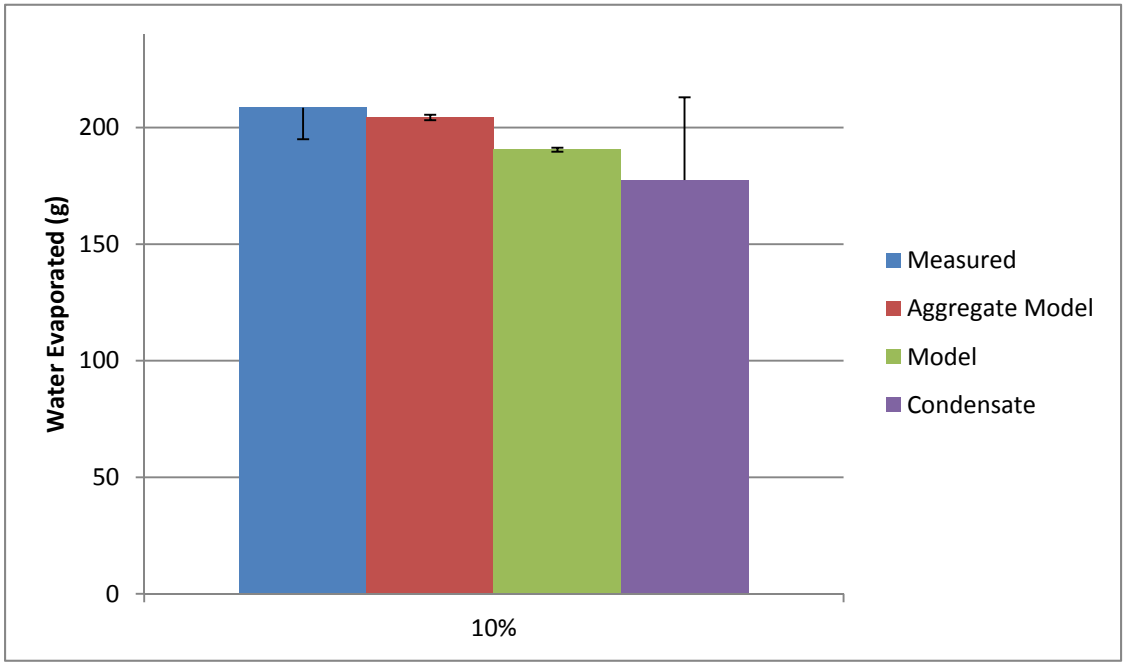

Figure 6-18: Comparison of Modeled and Measured Values of Evaporated Water for 10% Nominal Mass Fraction Solution

The first column, shown in blue, of Figure 6-18 is the amount of water determined by the difference in mass between the initial and final solutions states. The last column is the mass difference as measured by the condensate collected during regeneration. The red column is the amount predicted by the model calculated from the aggregate data from all three experiments and the green column is the predicted amount of water boiled from the individual test regression.

Above the columns are the errors associated with each measured value. As described in Section 5.6, the error bars above the "Measured" column represent the error determined by separate experiment associated with pouring the solution into and out of the evacuated tube. For the 10% solution this error is estimated at 13.5 grams as listed in Table 5-9. The error bars above the "Condensate" column represent a 20% uncertainty in the amount of water collected as condensate which is based on tests performed to determine the amount of water left in the condensing apparatus. In this case that is plus or minus 35.6 grams of water. It makes sense to think of the "Measured" and "Condensate" columns as bookends for the modeled values. This is because the bias error related to the "Measured" column push the uncertainty of that value greater that what it is in reality. The bias error associated with the "Condensate" value will always skew this measurement to under-predict the true value of water evaporated.

Figure 6-18 shows that for both the individual modeled regression and the aggregate regression, the amount of water evaporated falls between the two bookend values. Taking all of the Evaporated water values in conjunction with their associated uncertainties, it seems like the model predicts fairly well the amount of evaporated water for a 10% mass fraction solution.

Figure 6-19 shows the same breakdown of evaporated water values as Figure 6-18 for a 30% solution. In Figure 6-19 however, the values appear to be a little closer together. The error associated with the individual regression model incorporates both the mean measured value and the aggregate model value. Using the bias error of 28 grams, the condensate value can be seen to fall into the range of other values as well. The bias error included in the "Measured" value is estimated at 17.5 grams for this case.

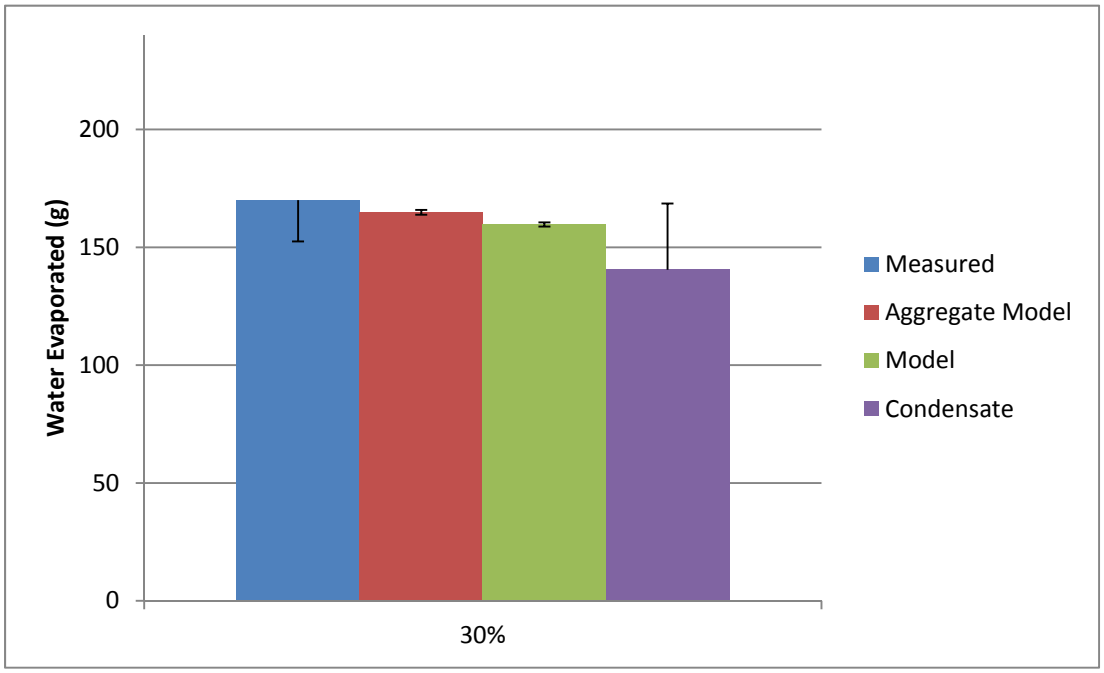

Figure 6-19: Comparison of Modeled and Measured Values of Evaporated Water for 30% Nominal Mass Fraction Solution

Figure 6-20 below shows the evaporated water values for a 50% solution. This chart again shows good agreement between the two modeled values, but in this case the modeled values fall closer to the mean value of the "Condensate" column as opposed to the "Measured" column. The bias error for the "Measured" value is 26 grams. The bias error from the "Condensate" measurement is 21.4 grams. The estimated error for the condensate values decreases as the solution mass fraction increases simply because the solution boiled inside the evacuated tube for a shorter period of time. This reduced boiling time was caused by the tube taking longer to reach boiling as the boiling point increased with an increase in solution mass fraction. The uncertainty with the "Measured" values increased with an increase in solution mass fraction due to the fact that the viscosity and surface tension of the solution increased with solution mass fraction.

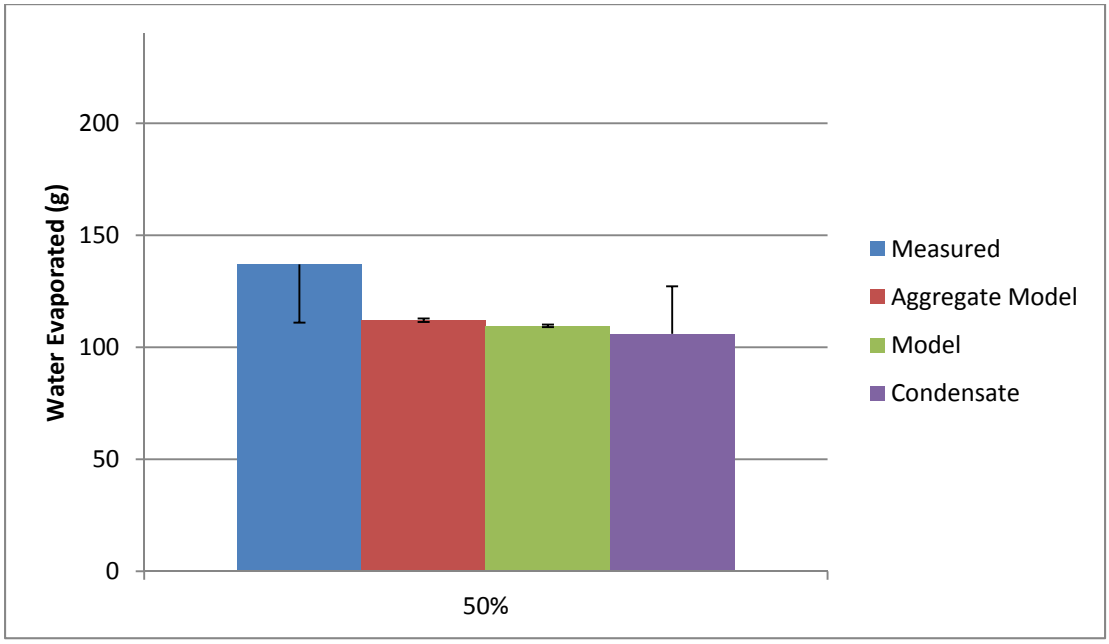

Figure 6-20: Comparison of Modeled and Measured Values of Evaporated Water for 50% Nominal Mass Fraction Solution

Overall, the amount of water predicted to be evaporated by the regression models falls between the values established as the upper and lower limits by the bias error of the "Measured" and "Condensate" values that were both directly measured. This is true for all three of the nominal mass fraction cases. This shows that not only can a liquid desiccant be regenerated in an evacuated tube to mass fractions above 50%, but regeneration performance can be predicted with a simple collector efficiency model.

7 CONCLUSIONS AND FUTURE WORK

7.1 Conclusion

This thesis shows that liquid desiccants can be regenerated in evacuated tube solar collectors. This is shown by direct measurement of a solution prior to and after boiling, analysis of the temperature and solar data collected during regeneration and the collection and measurement of water vapor during regeneration. These three methods of regeneration measurement give water evaporation rates that agree within the bounds of their statistical uncertainty. Also, at regeneration rates of around 0.65 kg/m2-hr, this technology is nearly three times as effective as Ghandidisan's closed solar still. These rates were only achieved once the solution came to a boil however and future testing of a steady state system would be needed to better compare the long term regeneration rates.

The ability to successfully regenerate liquid desiccants in evacuated tubes means that there is an efficient method of desiccant regeneration that is suitable for nearly all climate zones. Since water is forced off from the process of boiling and not standard mass transfer, this method of regeneration is not subject to poor performance in humid climates. Additionally, the highly insulating evacuated tube walls allow the regenerator to work in colder climates. The fact that the experiments took place after the autumnal equinox gives evidence to this statement.

It was also shown that regeneration performance can be predicted by using simple solar collector efficiency curves. This is an improvement over other desiccant regenerator models that rely on more complicated mass transfer relationships that can be difficult to adjust for climatic variances. The solar collector efficiency model is well understood and has been proven to work in a variety of situations. Being able to use this model to predict desiccant regeneration could significantly increase the possibility of evacuated tube desiccant regenerators being economically viable in the future.

7.2 Future Work

Future work includes taking the performance of a single tube and extrapolating this to the performance of an entire collector array. In addition to the array, work needs to be completed to better integrate this regeneration technology with desiccant heat pumps and air conditioners. Also, the simplified solar collector model should be integrated into a simulation program that can be used to predict the annual performance of evacuated tube desiccant regenerators. It would also be interesting to pursue analysis of why the different nominal mass fractions had slightly different performance curves.

8 REFERENCES

ASHRAE. *ANSI/ASHRAE Standard 93-2003, Methods of Testing to Determine the Thermal Performance of Solar Collectors.* Atlanta: American Society of Heating, Refrigeration and Air-Conditioning Engineers, Inc.

ASME. *Test Uncertainty, Part 1, ASME PTC 19.1-1998*. New York: American Society of Mechanical Engineers, Inc.

Budihardjo, I., G.. Morrison, and M. Behnia. 2007. Natural circulation flow through water-in-glass evacuated tube solar collectors. Solar Energy, 81, pp. 1460–1472.

Butler, G., and J. Beynon. 1967. The corrosion of mild steel in boiling salt solutions. Corrosion Science, Vol. 7, pp. 385-404.

Collier, R.K. 1979. The analysis and simulation of an open cycle absorption refrigeration system. Solar Energy, Volume 23, pp. 205-212.

Conde, M. 2004. Properties of aqueous solutions of lithium and calcium chlorides: formulations for use in air conditioning equipment design. International Journal of Thermal Sciences. Vol. 43, pp. 367-382.

Ertas, A., E. Anderson, and I. Kiris. 1992. Properties of new liquid desiccant solution – lithium chloride and calcium chloride mixture. Solar Energy, Volume 49, Issue 3, pp. 205-212.

Figliola, R.S., and D.E. Beasley. 2000. Theory and Design for Mechanical Measurements. New York: John Wiley & Sons, Inc.

Gandhidasan, P. 1983. Theoretical Study of a tilted solar still as a regenerator for liquid desiccants. Energy Conversion Management, Volume 23, Issue 2, Pages 97-101

Gandhidasan, P. 1984. Study of Roof Pond Liquid Desiccant System. Energy Research, Volume 8, Pages 387-392.

Gandhidasan, P. 1994. Performance Analysis of an Open cycle liquid desiccant cooling system using solar energy for regeneration. International Journal of Refrigeration . Vol. 17 No. 7.

Harding, G.L., Y. Zhiqiang, and D. Mackey. 1995. Heat extraction efficiency of a concentric glass tubular evacuated collector. Solar Energy, 35(1), pp. 71–9.

Kakabaev, A., and A. Khandurdyev. 1969. Absorption solar refrigeration unit with open regeneration of solution. Gelioteknika, 5(4), pp. 69-72.

Keenan, J.H., F.G Keyes, P.G. Hill, and J.G. Moore. 1969. Steam Tables. New York: John Wiley & Sons Inc.

Kim, Y, and T. Seo. 2007. Thermal performances comparisons of the glass evacuated tube solar collectors with shapes of absorber tube. Renewable Energy, Volume 32, Issue 5, Pages 772-795.

Kline, S.J., and F.A. McClintock. 1953. Describing uncertainties in single sample experiments. Mechanical Engineering, vol 75.

Lighthill, M.J. 1953. Theoretical considerations on free convection in tubes. Quarterly Journal of Mechanics and Applied Mathematics, 6, pp. 398–439.

Lipson, C., and Sheth, N. 1973. Statistical Design and Analysis of Engineering Experiments. New York: McGraw-Hill.

Morrison, G., I. Budihardjo, and M. Behnia. 2004. Water-in-glass evacuated tube solar water heaters. Solar Energy, 76, pp. 135-140.

Perez, R., P. Ineichen, R Seals, J Michalsky and R Stewart. 1990. Modeling daylight availability and irradiance components. Solar Energy, 44, pp. 277-289.

Perez, R., R. Seals, J. Anderson, and D. Menicucci. 1995. Calculating solar radiation received by tubular collectors. Journal of Solar Energy Engineering, 117 (4), pp. 341-344.

Perez, R., R. Seals, J. Anderson, and D. Menicucci. 1995. Calculating solar radiation received by tubular collectors. Journal of Solar Energy Engineering, 117, pp. 341-344.

Radhwan, A. M., H. Gari, and M. Elsayed. 1993. Parametric Study of a Packed Bed Dehumidifier/Regenerator Using CaCl Liquid Desiccant. Renewable Energy Vol. 3, No. 1. Pp. 49-60.

Reda, I., and A. Andreas. 2004. Solar position algorithm for solar radiation applications. Solar Energy, 76, pp. 577-589.

Theunissen, P.H., W.A. Beckman. 1985. Solar transmittance characteristics of evacuated tubular collectors with diffuse back reflectors. Solar Energy, Vol. 35, No. 4 , pp. 311-320.

Wheeler, A.J., and Ganji, A.R. 2004. Introduction to Engineering Experimentation. Upper Saddle River, New Jersey: Pearson Education, Inc.

Zhiqiang Y., G. Harding, and B. Window. 1984. Water-in-glass manifold for heat extraction from evacuated solar collector tubes. Solar Energy, 32(2), pp. 223–30.